THE SEARCH FOR ORBITAL DECAY IN HOT JUPITERS

by

Kishore Chandra Patra

Submitted to the Department of Physics
in partial fulfillment of the requirements for the degree of

Bachelor of Science in Physics

at the

MASSACHUSETTS INSTITUTE OF TECHNOLOGY

June 2018

© Massachusetts Institute of Technology 2018. All rights reserved.

Author ..... Signature redacted
Department of Physics
May 8, 2018

Certified by ..... Signature redacted
Nevin Weinberg
Associate Professor of Physics, MIT
Thesis Supervisor

Certified by ..... Signature redacted
Joshua N. Winn
Professor of Astrophysical Sciences, Princeton University
Thesis Supervisor

Accepted by .. Signature redacted
Scott H. Hughes
Interim Physics Associate Head, Department of Physics

MASSACHUSETTS INSTITUTE OF TECHNOLOGY
SEP 12 2018
LIBRARIES
ARCHIVES

MIT Libraries

77 Massachusetts Avenue
Cambridge, MA 02139
http://libraries.mit.edu/ask

DISCLAIMER NOTICE

The pagination in this thesis reflects how it was delivered to the Institute Archives and Special Collections.

Pages 85-86 are non-numbered blank pgs.

THE SEARCH FOR ORBITAL DECAY IN HOT JUPITERS

by

Kishore Chandra Patra

Submitted to the Department of Physics
on May 11, 2018, in partial fulfillment of the
requirements for the degree of
Bachelor of Science in Physics

Abstract

We summarize our results, so far, in the search for orbital decay in exoplanets. Orbital decay is the gradual shrinkage of the planetary orbit due to tidal dissipation. We ranked currently known exoplanetary systems according to the theoretical orbital decay rate and trimmed the list down to 12 best targets. We collected new transit light curves for the targets visible in the northern hemisphere using the 1.2 m telescope at the Fred L. Whipple Observatory, Arizona. For the southern targets, we are currently collaborating with the Las Cumbres Observatory Telescope Network to obtain new transits. We analyzed the timing residuals for each target, seeking evidence for any change in the orbital period.

Currently, the best candidate for orbital decay is WASP-12 b with an observed period derivative $\frac{dP}{dt} = -28 \pm 3$ ms yr^{-1}. However, we find that a few other possible models, including apsidal precession, nodal precession and color-dependent transit times, cannot be ruled out completely. Continous monitoring of WASP-12 b is necessary in the future to resolve the current conundrum. The search for orbital decay is still in its infancy for most other targets. However, we aim to produce a few transit times for each target to serve as an "anchor" for when TESS relays back more high quality light curves.

Thesis Supervisor: Nevin Weinberg
Title: Associate Professor of Physics, MIT

Thesis Supervisor: Joshua N. Winn
Title: Professor of Astrophysical Sciences, Princeton University

Acknowledgments

I would like to thank my advisors Professor Nevin Weinberg and Professor Josh Winn for providing me with support, guidance and exciting discussions throughout the duration of this project. Their help has been crucial to me at in understanding the scope and complexities of this project. I am also grateful to Liang Yu and Fei Dai, two graduate students at MIT who helped me with the computational aspects of this project including IDL, IRAF, python emcee and lmfit procedures. I would like to thank the team at Fred L Whipple Observatory and in particular, Allyson Bieryla for training me to use the 1.2 m telescope. Allyson also very kindly helped me retrieve some archival data from CfA. Thank you Matt Holman at CfA, the PI for Transit Light Curve Project, under which all observations at FLWO were carried out. I also thank Michael Gillon and Artem Burdanov for providing us light curves on WASP-19 and WASP-72 from the TRAPPIST telescope. I express the same gratitude towards Norio Narita and his team for helping us with the observations of WASP-12 simultaneously in different wavelengths. I would also like to thank Avi Shporer and the Las Cumbres Observatory Telescope Network for helping us with observing the southern targets. We look forward to a very successful collaboration in the future. I thank MIT Undergraduate Research Opportunities Program (UROP) department for supporting funding this project for a summer and two semesters. And thank you Sapna for bearing with my nocturnal working habits. This work would not have been possible without the help and support of all.

Contents

List of Figures

List of Tables

Chapter 1

Introduction

"*How vast those Orbs must be, and how inconsiderable this Earth, the Theatre upon which all our mighty Designs, all our Navigations, and all our Wars are transacted, is when compared to them. A very fit consideration, and matter of Reflection, for those Kings and Princes who sacrifice the Lives of so many People, only to flatter their Ambition in being Masters of some pitiful corner of this small Spot.*"

- Christiaan Huygens, The Cosmotheoros of Christiaan Huygens (1698) Book II

The first exoplanet orbiting a main sequence star was discovered more than 20 years ago (Mayor and Queloz 1995). Since then, the NASA Exoplanet Archive has recorded more than 3700 (as of Feruary 15 2018) confirmed exoplanets and nearly 4500 Kepler candidates. A vast majority of these exoplanets have been discovered via the transit method, thanks to the Kepler and K2 Space Mission. An exoplanet transit happens when a planet crosses in front of the face of a star, dimming the star's brightness momentarily (see Winn 2010). The first full exoplanet transit was detected in the year 2000 in the system HD 209458 (see Charbonneau et al. 2000 and Henry et al. 1999). Since the detection signal in transit surveys is proportional to the ratio of cross-sectional area of the planet to that of the star's, the transit method preferentially discovers giant planets in tight orbits around their stars. Being so close to their host stars, these planets can have temperatures up to 2300 K (Harrington et al. 2007) and hence are appropriately called "hot Jupiters". While not the ideal laboratories for the search of extraterrestrial life, these hot Jupiters play a crucial part in our understanding

of the planet formation theories and planetary dynamics. This work explores one of the dynamical result of planet-star interactions from a close distance, namely the orbital decay of exoplanets.

1.1 Orbital Decay In Exoplanets

Orbital decay refers to the gradual shrinkage of a planetary orbit, leading ultimately to the engulfment of the planet by its host star (see Rasio et al. 1996; Sasselov 2003; Levrard et al. 2009). Stars and close-in hot Jupiters can be considered extended fluid bodies. These bodies tend to be non-spherical because of their rotation and tidal deformation due to the variation in gravitational force across the extent of the bodies. These tides are responsible for continuously changing the system's orbital and rotational parameters. When the rotational velocity ω of the star is much smaller than the orbital velocity Ω of a close-in planet, the tidal bulge in the star lags behind the orbiting planet as shown in Figure 1-1. As a result, friction is generated between the moving tides and the convective layers of the star. The dissipative nature of the tidal friction causes loss of total energy of the system. Angular momentum is still conserved, though it may be exchanged between the bodies. For a star-planet system with $\Omega \gg \omega$, angular momentum is transferred from the orbit to stellar spin. Over time, the planet's orbit is expected to shrink and the star is expected to spin faster.

Hut (1980) showed that if a binary star-planet system has a total angular momentum ($L_t = L_s + L_o$), which is the sum of planet's orbital angular momentum and star's spin angular momentum, less than a critical angular momentum (L_c), then tidal evolution leads to a decaying orbit of the planet. Such a system is called "Darwin-unstable". Using numerical simulations, it has been predicted that (see Figure 1 of Levrard et al. 2009) most of the known hot Jupiters are Darwin-unstable and should be undergoing continual orbital decay, rather than approaching a stable equilibrium orbit.

Despite the firm theoretical prediction and the relative abundance of Darwin-unstable systems, a shrinking orbit of an exoplanet has never been securely detected. Orbital decay is often invoked to explain ensemble properties of hot Jupiters like scarcity of gas giants with period less than a day (see Jackson et al. 2008; Hansen 2010; Penev et al. 2012;

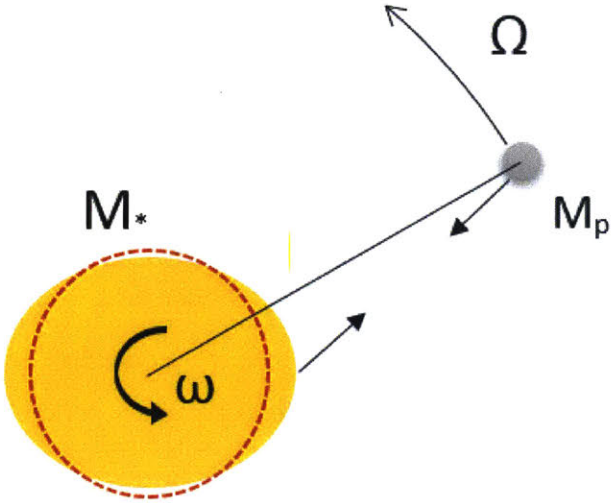

Figure 1-1: When Ω is $\gg$ than ω, the tidal bulge raised on star lags behind.

Ogilvie 2014), anomalously rapid rotation of some hot-Jupiter host stars (see Penev et al. 2016), absence of hot Jupiters around subgiant stars (see Villaver & Livio 2009; Hansen 2010; Schlaufman & Winn 2013), lower occurrence of close-in planets around rapidly rotating stars (Teitler & Konigl 2014) and the realignment of stars and their planetary orbits (Matsakos & Konigl 2015). However, there is no convincing evidence for actual shrinkage of an exoplanet's orbit due to tidal dissipation (see for e.g. Hoyer et al. 2016; Wilkins et al. 2017).

Part of the problem is that the theory does not confidently predict the rate and consequently the timescale of orbital decay. The tide raised by a hot Jupiter can excite large amplitude waves within its host star. These waves transfer energy and angular momentum from the planet's orbit to the star resulting in a gradual in-spiral of the planet. The rate of orbital decay is then determined by the efficiency of tidal dissipation and depends on the amplitude of the waves as well as the effectiveness of frictional processes within the star (adapted from Essick & Weinberg 2016). Tidal dissipation is parametrized by the stellar tidal quality parameter $Q_\star$, a dimensionless number defined as the ratio of energy in the orbit to the work done by internal friction in each orbital cycle (a larger $Q_\star$ implies less dissipation). A generally accepted value of $Q_\star \sim 10^6$ comes from the observed circularization

rate of solar-type binaries (Meibom & Mathieu 2005). However, because $Q_\star$ is not a fundamental property of the star but depends on the shape and size of the orbit and the mass of the perturber, $Q_\star$ may not necessarily be $\sim 10^6$, leading to uncertainty and confusion over range of values of $Q_\star$ found in the literature.

Based on the generally accepted value of $Q_\star \sim 10^6$, it has been estimated that it would require observations spanning ~10 years to securely detect any shrinkage in a typical hot Jupiter's orbital period (see Birkby 2014). This presents the second major challenge in detecting orbital decay. High-precision transit times are required at regular intervals over a period of ten years or more to discern any long term trends in period.

1.2 Transit Timing

Transit photometry depends on the physical obstruction of star's light by a planet. An example schematic of a transit and the corresponding light curve is shown in Figure 1-2. A host of planetary parameters can be determined from a light curve, including the orbital period P, semi-major axis a, impact paramater b, orbital inclination i, ratio of planet's radius to star's radius $R_p/R_\star$ etc. (see Winn 2011 for more details). For detecting orbital decay, the parameter orbital period is the most important, which can be determined by observing a sequence of transits, and fitting a linear function

$$t_c(n) = t_c(0) + nP \tag{1.1}$$

where $t_c(n)$ is the time of conjuntion of the n^{th} transit. The choice of 0^{th} transit is arbitrary but is typically chosen to be near the middle of observational baseline. The error in transit period is inversely proportional to the number of observed transits over time, resulting in highly precise periods down to 10^{-8} days. However care must be taken to ensure a consistent time-stamp for all transits. For exoplanet transits, it is advisable to work with the Barycentric Dynamical Time (BJD_{TDB}) which corrects for relativistic time dilation and is uniform time as one would measure from earth if it were not moving around the sun.

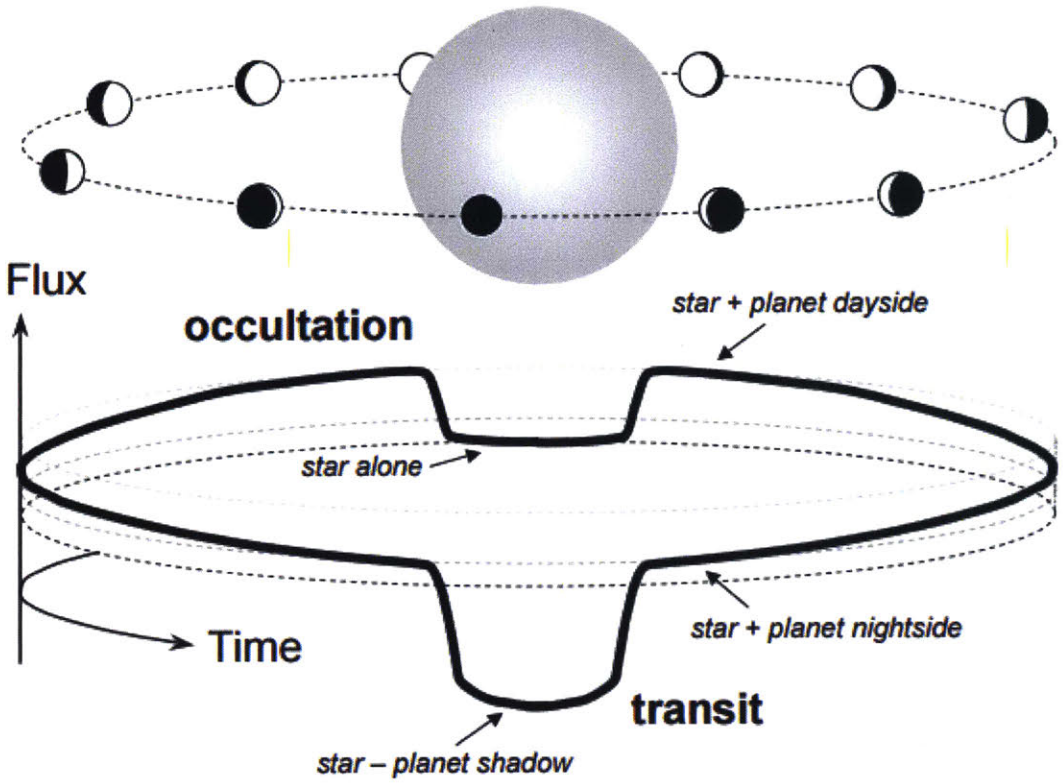

Figure 1-2: Flux of star as a function of planet's orbital phase. Image courtesy of J. Winn 2011, from *Transits and Occultations*

1.3 Ranking Of Targets

In presenting the theoretical framework for orbital decay, Levrard et al. (2009) found that the remaining time for the planet to reach its host star from an initial orbital distance a is

$$\tau \approx \frac{P}{48}\frac{Q_*}{2\pi}\left(\frac{a}{R_*}\right)^5 \frac{M_\star}{M_\mathrm{p}} \tag{1.2}$$

From the work of Laskar et al. (1997), one can find a simplified expression for the short-term rate of change of period, assuming that stellar rotational frequency is much smaller than the planet's orbital frequency,

$$\frac{dP}{dt} = -\frac{27\pi}{2Q_\star}\left(\frac{R_\star}{a}\right)^5 \frac{M_\mathrm{p}}{M_\star} \tag{1.3}$$

1.3 shows that the best targets to investigate are the ones with small semi-major axis, large stellar radius and high mass. We sorted the list of exoplanets taken from the online database *exoplanets.org* and sorted them according to the value of ϕ where we define ϕ as

$$\phi \equiv \left(\frac{R_*}{a}\right)^5 \frac{M_\mathrm{p}}{M_*} \tag{1.4}$$

Assuming a $Q_* \sim 10^6$, a nominal decay timescale was determined for each potential target.

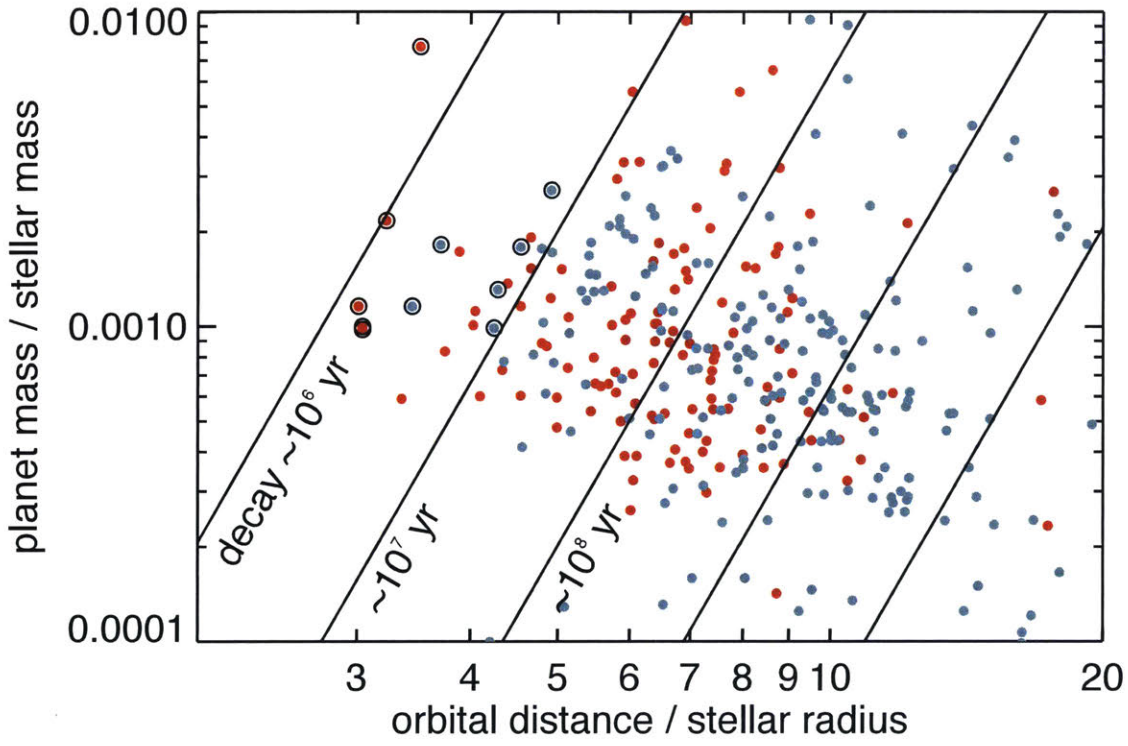

Figure 1-3: The predicted orbital decay timescales for the best targets. The blue dots are for stars for $T_{\mathrm{eff}} < 6000$ K and red dots are the hotter stars. Image courtesy: J.N. Winn

Planet	RA	DEC	Vmag	T_{eff} [K]	N_{obs}	Expected $\frac{dP}{dt}$ [ms/year]	Ref.
WASP-18 b	01:37:25	-45:40:40	9.3	6400 ± 100	0	-24	Hellier et al. 2011
KELT-16 b	20:57:04	31:39:40	11.7	6236 ± 54	2	-11	Oberst et al. 2017
WASP-103 b	16:37:16	07:11:00	12.1	6110 ± 160	4	-9	Gillon et al. 2014
OGLE-TR-56 b	17:56:35	-29:32:21	16.6	5900 ± 80	0	-3	Sasselov 2003
WASP-12 b	06:30:33	29:40:20	11.7	6300 ± 150	13	-6	Hebb et al. 2009
HATS-18 b	11:35:50	-29:09:22	14.1	5600 ±120	0	-5	Penev et al. 2016
WASP-19 b	09:53:40	-45:39:33	12.6	5500 ± 100	3	-4	Hebb et al. 2010
WASP-43 b	10:19:38	-09:48:23	12.4	4400 ± 200	0	-2	Hellier et al. 2011
HAT-P-23 b	20:24:30	16:45:44	12.4	5905 ± 80	3	-4	Bakos et al. 2011
WASP-114 b	21:50:40	10:27:47	12.7	5940 ± 140	2	-2	Barros et a. 2016
WASP-122 b	07:13:12	-42:24:35	11.0	5720 ± 130	0	-1	Turner et al. 2016
WASP-72 b	02:44:10	-30:10:09	10.9	6250 ± 100	2	-2	Gillon et al. 2013

Table 1.1: The 12 best targets for the search of orbital decay. N_{obs} is the number of high-quality light curves used for this project. Expected $\frac{dP}{dt}$ is calculated using equation 1.3 and assuming $Q_* \sim 10^6$

Table 1.1, lists the best 12 targets according to our metric ϕ. Our list of targets also includes a few newly discovered exoplanets that do not currently have a long observational baseline. The goal for these "new" exoplanets is to set up a pedestal for future follow-up work in the search for orbital decay. Another important consideration into the target selection was the effective temperature, T_{eff} of the star. Theoretically, orbital decay depends on the efficiency of tidal dissipation in the thick convective zones within the stellar interior. Cooler stars with $T_{eff} < 6000$ K, as opposed to hotter stars, are expected to have such thick convective zones, although much uncertainty and lack of observational evidence remain for the relation between tidal dissipation and stellar interior structure. Therefore, we have included a few hotter stars in our list to serve as a "control group" to aid future tests for theories of tidal dissipation.

Chapter 2

Data Collection And Analysis

2.1 Image Processing And New Transit Times

Light curves for the targets observable in the northern hemisphere were obtained from the 1.2 m reflector telescope at the Fred L. Whipple Observatory (FLWO) in Arizona, USA. Images were obtained at FLWO with the KeplerCam detector through a Sloan r'-band filter. The field of view of this camera is $23'.1$ on a side. We used 2×2 binning, giving a pixel scale of $0''.68$. In a recent collaboration, some southern targets will be observed under the Key Project at the Las Cumbres Observatory (LCO) telescope network starting January 2018. We are currently using the 1.0 m telescopes at Cerro Tololo Inter-American Observatory (CTIO) in Chile, Siding Spring Observatory (SSO) in Australia and South African Astronomical Observatory (SAAO). Each of these telescopes is installed with the same Sinistro CCD with a FoV $27' \times 27'$ and a pixel scale of $0''.39$. The LCO collaboration is still in its infancy and is expected to result in several transits of southern targets in the future. We also collaborated with Michael Gillon et al. for WASP-19 light curves obtained with the TRAPPIST telescope at Observatorio La Silla, Chile. Details on individual observations including date of observation, exposure time and filter are provided in Section 2.2.

The raw images were processed by performing standard overscan correction, debiasing, and flat-fielding with IRAF. [1] Aperture photometry was performed for each target and an

[1]The Image Reduction and Analysis Facility (IRAF) is distributed by the National Optical Astronomy Observatory, which is operated by the Association of Universities for Research in Astronomy (AURA) under a cooperative agreement with the National Science Foundation.

ensemble of 7-9 comparison stars of similar brightness. Aperture radius was chosen to give the smallest scatter in the flux outside of the transits. The reference signal was generated by summing the flux of the comparison stars. The flux of the target star was then divided by this reference signal to produce a time series of relative flux. Each time series was normalized to have unit flux outside of the transit. The time stamps were placed on the BJD_{TDB} system using the code of Eastman et al. (2010). We fitted a Mandel & Agol (2002) model to the data from each transit. The parameters of the transit model were the mid-transit time, the planet-to-star radius ratio (R_p/R_*), the scaled stellar radius (R_*/a), and the impact parameter ($b = a\ cos(i)/R_*$). For given values of $R_*/a$and b, the transit timescale is proportional to the orbital period (see, e.g., Equation (19) of Winn 2010). To set this timescale, we held the period fixed at its most recent measurement for each target exoplanet, although the individual transits were fitted separately with no requirement for periodicity. To correct for differential extinction, we allowed the apparent magnitude to be a linear function of airmass, giving two additional parameters. The limb darkening law was assumed to be quadratic, with coefficients held fixed at the values tabulated by Claret & Bloemen (2011) for each target star.

To determine the credible intervals for the parameters, we used the emcee Markov Chain Monte Carlo (MCMC) code written by Foreman-Mackey et al. (2013). The transition distribution was proportional to exp(-$\chi^2/2$) with

$$\chi^2 = \sum_{i=1}^{N} \left(\frac{f_{obs,i} - f_{calc,i}}{\sigma_i} \right)^2 \tag{2.1}$$

where $f_{obs,i}$ is the observed flux at time t_i and $f_{calc,i}$ is the corresponding flux of the model. The uncertainties σ_i were set equal to the standard deviation of the out-of-transit data. In a few cases, the pre-ingress scatter was noticeably different than the post-egress scatter; for those observations, we assigned σ_i by linear interpolation between the pre-ingress and post-egress values.

2.2 Timing Analysis For All Targets

For each target, we included all of the transit times we could find in the literature for which (i) the analysis was based on observations of a single event, (ii) the midpoint was allowed to be a completely free parameter, (iii) the time system is documented clearly, (iv) the light curve includes both ingress and egress.

We fitted two models to the timing data using the MCMC method. The first model assumes a circular orbit and a constant orbital period

$$t_{tra}(E) = t_0 + PE, \tag{2.2}$$

where E is the epoch number and P is the period. Next, we fitted a model that assumes a circular orbit and a constant period derivative

$$t_{tra}(E) = t_0 + PE + \frac{1}{2}\frac{dP}{dE}E^2, \tag{2.3}$$

from which the implied period derivative is

$$\frac{dP}{dt} = \frac{1}{P}\frac{dP}{dE} \tag{2.4}$$

The following subsections summarize the fitting of above models to each target and present the implied lower limits on the tidal quality parameter Q_*.

2.2.1 WASP-18 b

WASP-18 b is a heavy hot Jupiter with a mass of $\sim 10 M_J$ in a 0.94 day orbit around a relatively hot F6 type star (Hellier et al. 2011). Despite being discovered in 2009, WASP-18 b has not been regularly observed because of its location in the far southern sky. For this project, we do not have any new transits yet. However, collaborating with the LCO Key Project, we are scheduled to obtain 5-6 new transits in the upcoming season of June-September 2018.

McDonald and Kerins (2018) found a weak 1.3σ evidence for orbital decay in WASP-18 b

after appending post-discovery transit times with a pre-discovery transit seen by Hipparcos (see McDonald and Kerins (2018) for more details). The implied tidal quality factor is $Q_* \sim 5 \times 10^5$, lower than the typical range of $10^{6\text{-}7}$ inferred from ensemble analyses of binary stars and star-planet systems (see, e.g., Meibom & Mathieu 2005; Hansen 2010; Penev et al. 2012). WASP-18 b is still a prime candidate for the detection of orbital decay and warrants consistent transit observations in the future.

2.2.2 KELT-16 b

KELT-16 b is a ~ 2.8 M_J planet in 0.97 day orbit (Oberst et al. 2016). Since its discovery in 2016, the following two light curves, obtained for this project at FLWO in r' filter, are the only follow-up observations available. Table 2.1 summarizes the observation details and the measured mid-transit times.

Target	Epoch	Date-Obs UTC	Exp (sec)	T_{mid} BJD_{TDB}	Unc (days)
KELT-16 b	773	2017-June-10	30	2457914.88516	0.00081
KELT-16 b	774	2017-June-11	30	2457915.85393	0.00062

Table 2.1: Observation journal for KELT-16 and calculated mid-transit times.

Figures 2-1 and 2-2 show the new light curves and timing residuals respectively. The black circles in Fig. 2-2 are all the observations of KELT-16 by Oberst et al. in the discovery paper. Currently, we are unable to draw any conclusion on orbital decay despite the apparent quadratic fit to the timing residuals. Data over a longer time baseline are required to confirm whether the orbit of KELT-16 is indeed decaying.

Based on the current data at hand, the orbital decay model implies a period derivative

$$\frac{dP}{dt} = \frac{1}{P}\frac{dP}{dE} = -30 \pm 31 \text{ms yr}^{-1}. \tag{2.5}$$

which is consistent with a constant period. Using Equation 1.3, we can put a 2σ lower limit on $Q_* > 4 \times 10^4$.

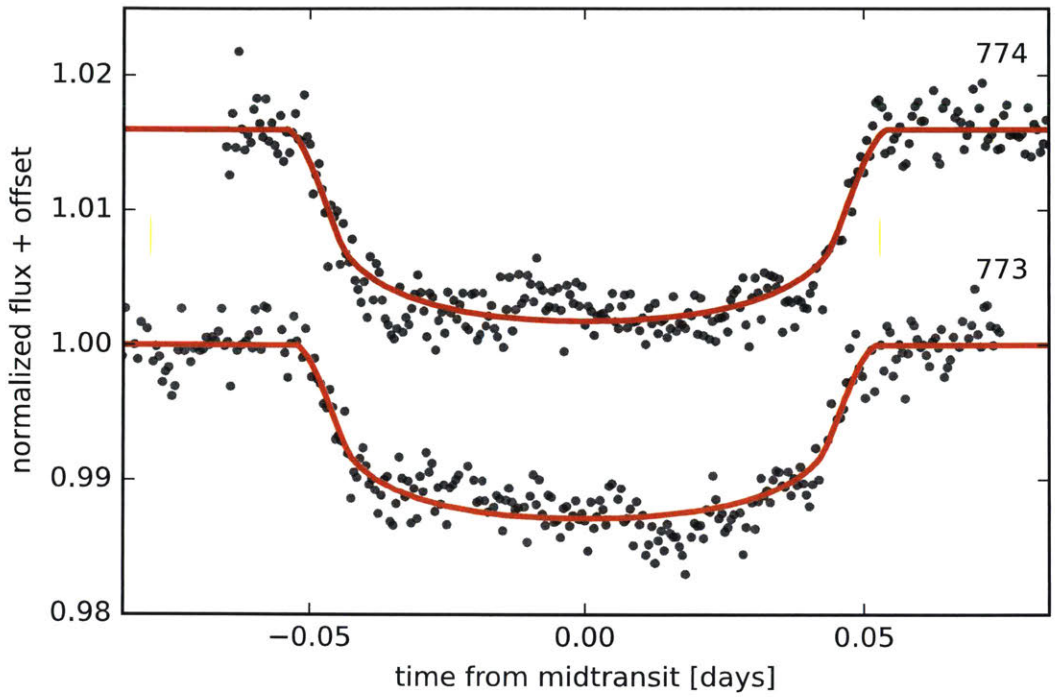

Figure 2-1: New transit light curves for KELT-16 b. Epoch numbers are printed to the right of each curve. Vertical offsets have been applied to separate the light curves.

2.2.3 WASP-103 b

WASP-103 b is a $\sim$ 1.5 M_J planet in 0.93 day orbit (Gillon et al. 2014). New data were obtained for WASP-103 b at FLWO in r' filter. Table 2.2 summarizes the observation details and the measured mid-transit times.

Figures 2-3 and 2-4 show the new light curves and timing residuals respectively. Like KELT-16 b, we are unable to draw any conclusion on orbital decay despite the apparent quadratic fit to the timing residuals. Data over a longer time baseline are required to confirm whether the orbit of WASP-103 b is indeed decaying.

Based on the current data at hand, the orbital decay model implies a period derivative

$$\frac{dP}{dt} = \frac{1}{P}\frac{dP}{dE} = -34 \pm 27\text{ms yr}^{-1}. \tag{2.6}$$

The period derivative is consistent with a constant period. Using Equation 1.3, we can put

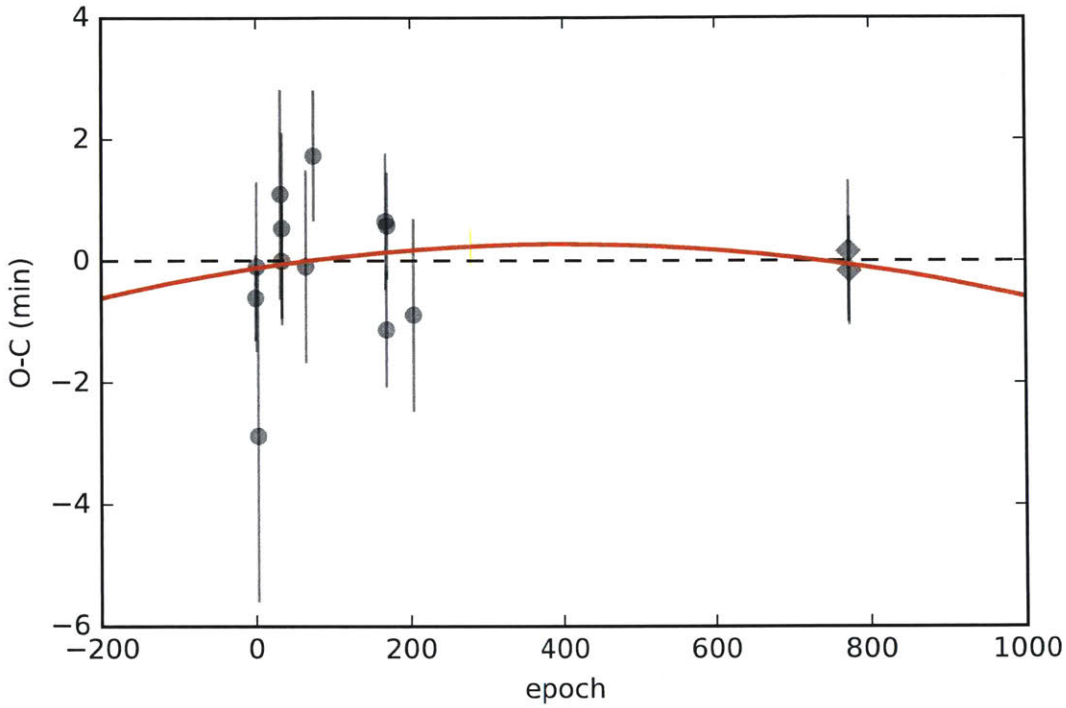

Figure 2-2: Timing residuals for KELT-16 b. The black circles are previously reported transit times and the black diamonds are new transit times obtained for this work. The red line is the best-fit orbital decay model.

a 2σ lower limit on $Q_* > 4 \times 10^4$.

2.2.4 OGLE-TR-56 b

OGLE-TR-56 b is perhaps the most difficult target in our list to observe. Only visible in the southern sky, OGLE-TR-56 is a dim star with a V_{mag} 16.6 requiring a larger telescope than 1.2 m at FLWO for a decent signal-to-noise ratio on its brightness measurement. Nevertheless, it is also the earliest discovered exoplanet (discovered in 2003) in our list, making it a prime candidate for future observations in the search for orbital decay, on the basis of having a close to 15 year time baseline since discovery. We currently do not have new observations of OGLE-TR-56 for this project.

Target	Epoch	Date-Obs UTC	Exp (sec)	T_{mid} BJD_{TDB}	Unc (days)
WASP-103 b	731	2016-May-04	30	2457512.87006	0.00031
WASP-103 b	759	2016-May-30	30	2457538.78548	0.00030
WASP-103 b	773	2016-Jun-12	30	2457551.74314	0.00038
WASP-103 b	1107	2017-Apr-17	30	2457860.87503	0.00029

Table 2.2: Observation journal for WASP-103 and calculated mid-transit times.

2.2.5 WASP-12 b

WASP-12 b is currently the best candidate for the detection of orbital decay (see Chapter 3 for a detailed analysis of WASP-12 b). It is a ~ 1.4 M_J planet in 1.09 day orbit (Hebb et al. 2009). Maciejewski et al. (2016) reported the first hint of WASP-12's deviation from linear ephemeris. Since then, we have collected two new seasons worth of transit times. Table 2.3 summarizes the observation details and the measured mid-transit times of the latest 2017-2018 observation season.

Target	Epoch	Date-Obs UTC	Exp (sec)	T_{mid} BJD_{TDB}	Unc (days)
WASP-12 b	3270	2017 Nov 20	14	2458077.92107	0.00028
WASP-12 b	3312	2018 Jan 05	12	2458123.76011	0.00027
WASP-12 b	3313	2018 Jan 06	12	2458124.85183	0.00035
WASP-12 b	3322	2018 Jan 16	12	2458134.67471	0.00032
WASP-12 b	3324	2018 Jan 18	12	2458136.85760	0.00033
WASP-12 b	3345	2018 Feb 10	12	2458159.77773	0.00091

Table 2.3: Observation journal for WASP-12 and calculated mid-transit times.

Figures 2-5 and 2-6 show the new light curves and timing residuals respectively. While visually, the orbital decay model looks convincing, an apsidal precession model cannot be ruled out either. These competing models are discussed in detail in Chapter 3.
Based on the current data at hand, the orbital decay model implies a period derivative

$$\frac{dP}{dt} = \frac{1}{P}\frac{dP}{dE} = -28 \pm 3\text{ms yr}^{-1}. \tag{2.7}$$

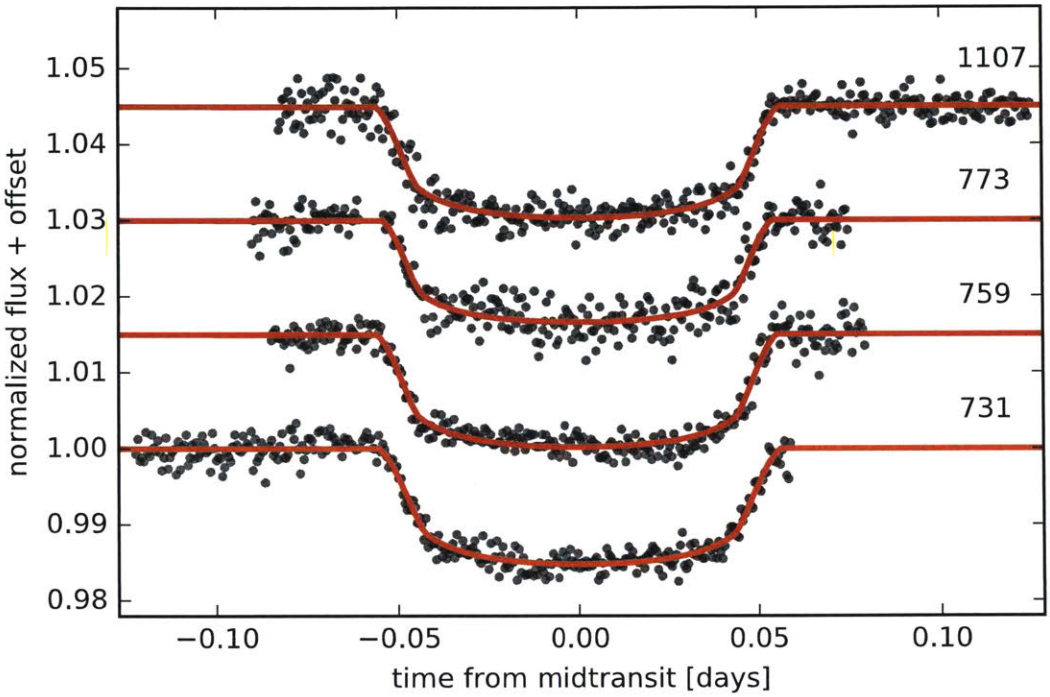

Figure 2-3: New transit light curves for WASP-103 b. Epoch numbers are printed to the right of each curve. Vertical offsets have been applied to separate the light curves.

The orbital decay model implies $Q_* \sim 2 \times 10^5$. We continue to monitor WASP-12 b with a high priority.

2.2.6 HATS-18 b

HATS-18 b is a ~ 2.0 M_J planet in 0.84 day orbit around its star. It was recently discovered in 2016 by Penev et al. Currently, we do not have any follow-up observations of HATS-18 b, though we are scheduled to carry out new observations from the LCO Telescope Network next season starting January 2019.

2.2.7 WASP-19 b

WASP-19 b was discovered in 2010 by Hebb et al. It is a ~ 1.1 M_J planet in 0.78 day orbit around its star. New data were obtained for WASP-19 b by Gillon et al. in $I + z$ filter using

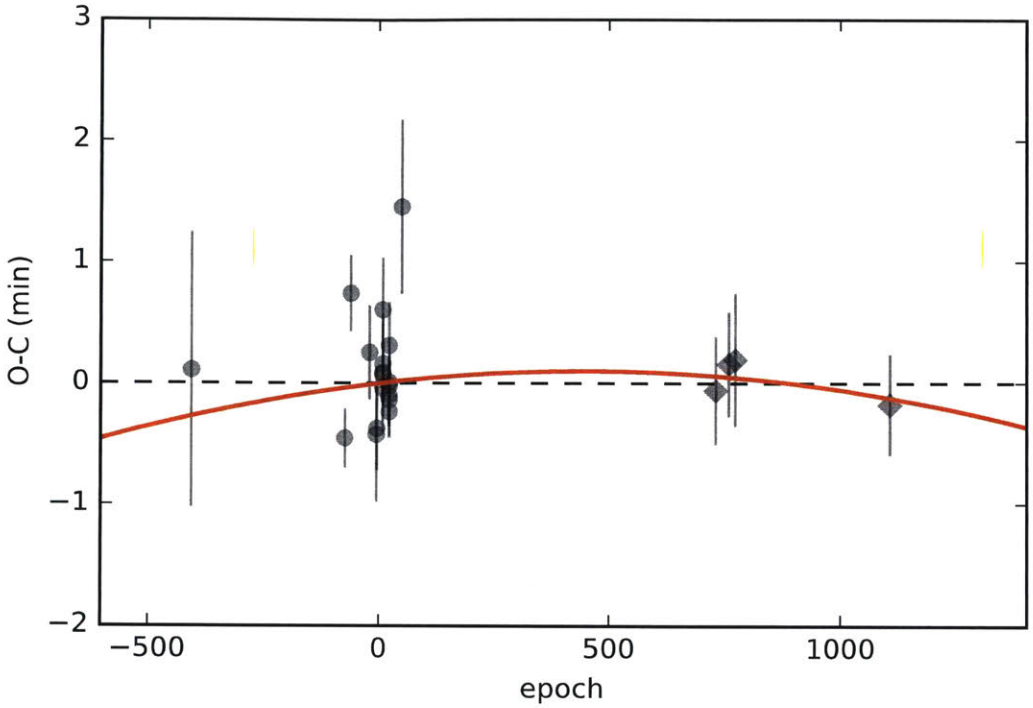

Figure 2-4: Timing residuals for WASP-103 b. The black circles are previously reported transit times and the black diamonds are new transit times obtained for this work. The red line is the best-fit orbital decay model.

the TRAPPIST telescope in La Silla ESO Observatory, Chile. Table 2.4 summarizes the observation details and the measured mid-transit times

Figures 2-7 and 2-8 show the new light curves and timing residuals respectively. WASP-19 is closing on a decade since discovery which makes it a promising candidate for the detection of orbital decay in the near future. Current data are not sufficient enough to confirm a decaying orbit despite a negative period derivative. Based on the current data at hand, the orbital decay model implies a period derivative

$$\frac{dP}{dt} = \frac{1}{P}\frac{dP}{dE} = -12 \pm 7\text{ms yr}^{-1}. \tag{2.8}$$

Using Equation 1.3, we can put a 2σ lower limit on $Q_* > 2 \times 10^5$.

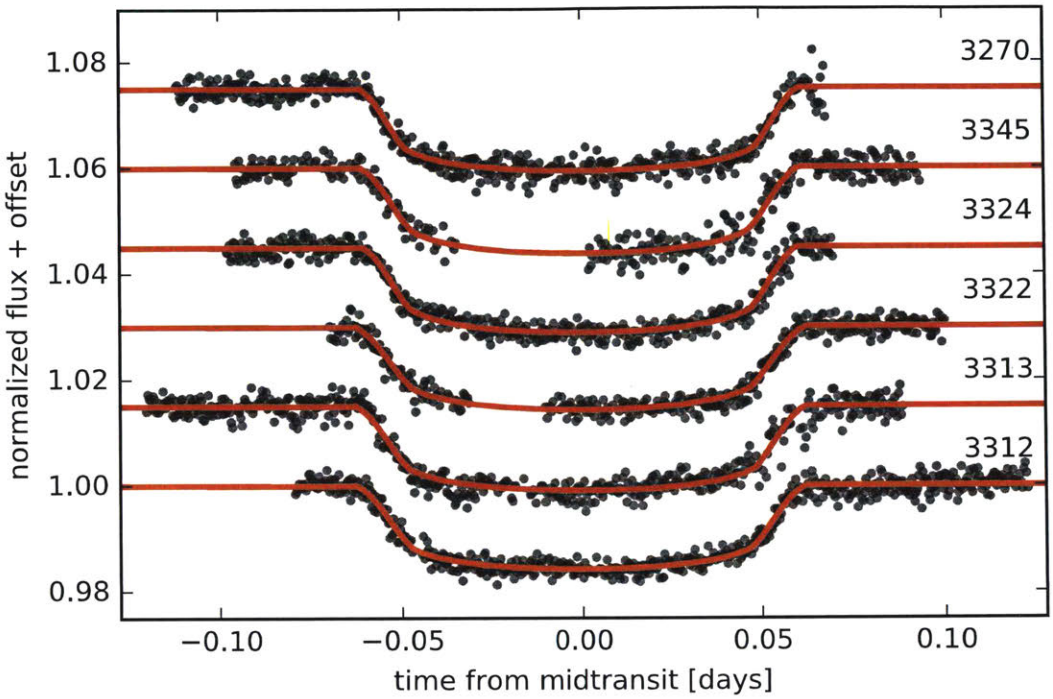

Figure 2-5: New transit light curves for WASP-12 b. Epoch numbers are printed to the right of each curve. Vertical offsets have been applied to separate the light curves.

2.2.8 WASP-43 b

WASP-43 b, a ~ 2 M_J planet in a 0.8 day orbit was discovered in 2011 by Hellier et al. Since then, it has had somewhat of a tumultuous journey as far as orbital decay is concerned. In 2016, Jiang et al. claimed a detection of orbital decay in WASP-43 b with $\frac{dP}{dt} = -29 \pm 7$ ms yr^{-1}, which would be a nearly 4σ detection. However, in the same year, Hoyer et al. (2016) ruled out orbital decay by presenting more transits that were consistent with a constant period. They also put a limit on $Q_* > 10^5$. We have not collected new transits for WASP-43 since 2016, though we have older transits available. We plan on obtaining new transits on WASP-43 b in the future using the 1.2 m telescope at FLWO and also re-analyzing all the older light curves in the meanwhile.

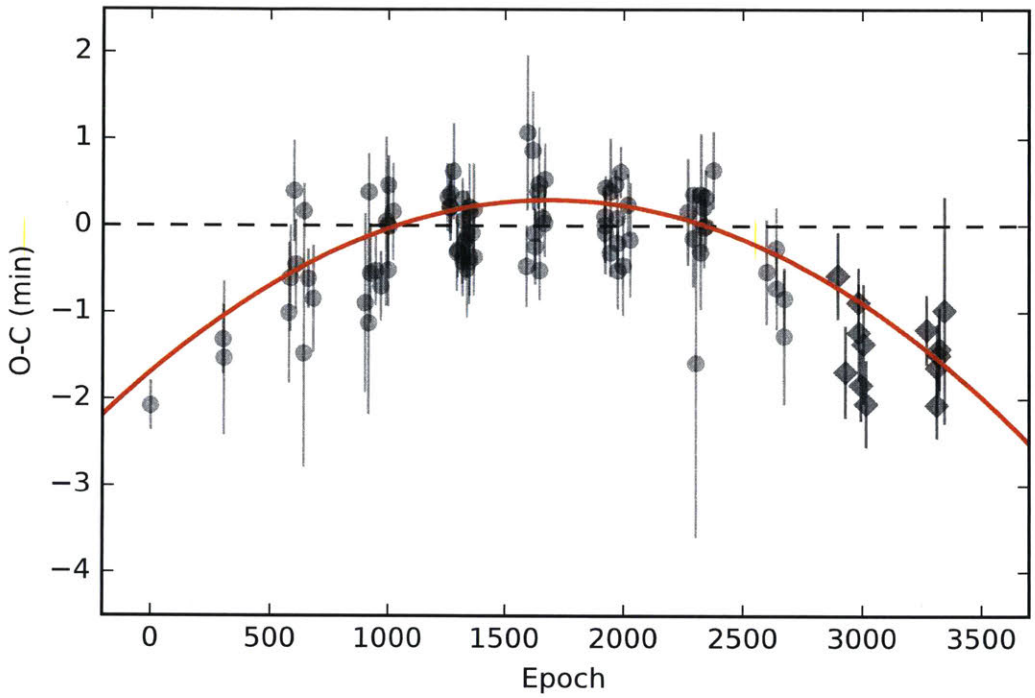

Figure 2-6: Timing residuals for WASP-12 b. The black circles are previously reported transit times and the black diamonds are new transit times obtained for this work.

2.2.9 HAT-P-23 b

HAT-P-23 b is a $\sim$ 2.1 M_J planet in a 1.2 day orbit around its star (Bakos et al. 2010). We observed 3 new transits at FLWO in r' filter. Table 2.5 summarizes the observation details. Figures 2-9 and 2-10 show the new light curves and the timing residuals respectively.

The new timing residuals of HAT-P-23 b are surprising. The best-fit orbital decay model to the timing residuals has a positive period derivative that implies the orbit is expanding rather than shrinking as predicted by the theory. However, it can be seen that this orbital decay model is quite a poor fit to points between epochs 500 and 1200, suggesting that orbital decay model may not be the best interpretation of the timing residuals. One potential reason for the positive deviation of new transit times is the occultation of starspots by the planet which may throw off transit times. While a weak bump can be seen in some of the light curves in Fig. 2-9, it is not convincing enough at the current noise level to definitively attribute

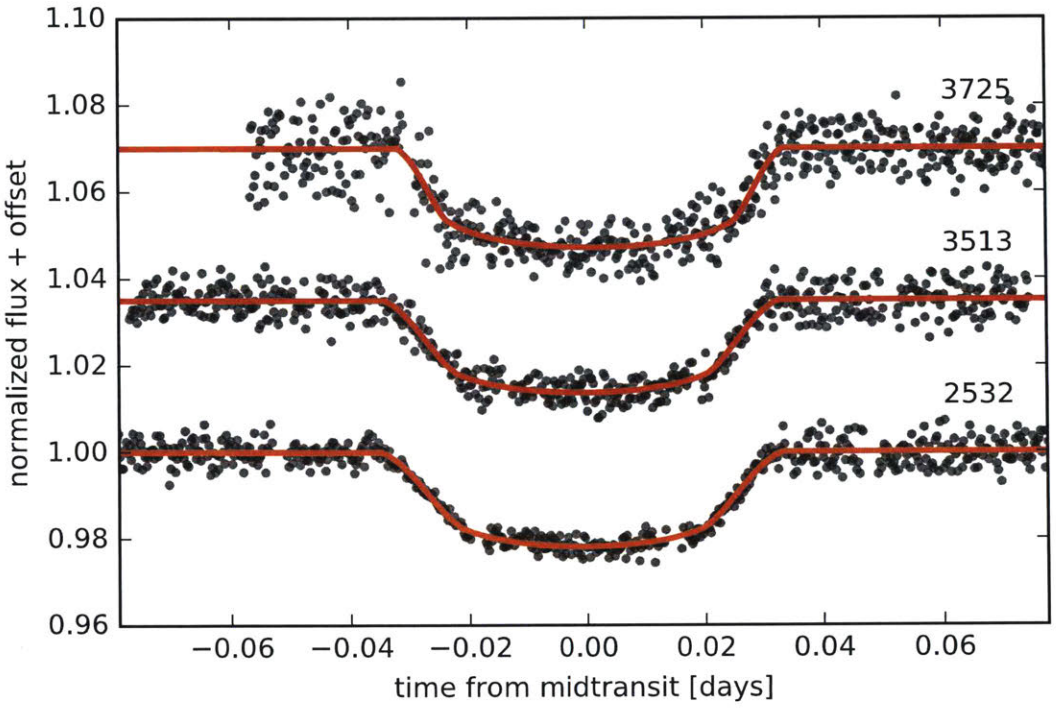

Figure 2-7: New transit light curves for WASP-19 b. Epoch numbers are printed to the right of each curve. Vertical offsets have been applied to separate the light curves.

Target	Epoch	Date-Obs UTC	Exp (sec)	T_{mid} BJD_{TDB}	Unc (days)
WASP-19 b	2532	2014 Apr 25	12	2456772.67789	0.00042
WASP-19 b	3513	2016 Jun 07	12	2457546.52955	0.00038
WASP-19 b	3725	2016 Nov 21	12	2457713.76203	0.00031

Table 2.4: Observation journal for WASP-19 b and calculated mid-transit times.

Target	Epoch	Date-Obs UTC	Exp (sec)	T_{mid} BJD_{TDB}	Unc (days)
HAT-P-23 b	2299	2016 Sep 09	20	2457640.69114	0.00046
HAT-P-23 b	2313	2016 Sep 26	20	2457657.67134	0.00062
HAT-P-23 b	2318	2016 Oct 02	20	2457663.73660	0.00044

Table 2.5: Observation journal for HAT-P-23 b and calculated mid-transit times.

this timing anomaly to starspots. A study of transit times simultaneously in different filters might help test for the effect of starspots on transit times for HAT-P-23 b (see Chapter 4, section 1 for an example of similar analysis for WASP-12 b). Bakos et al. (2010) report an eccentric orbit with $e = 0.106 \pm 0.044$, which opens an avenue for another possible model for transit times, namely apsidal precession of orbit (see Chapter 3 for more details on apsidal precession and Chapter 5 for a brief study of eccentricity of HAT-P-23). However a non-zero eccentricity in a short-period hot Jupiter contradicts the rapid tidal circularization theory (Goldreich & Soter, 1966). In any case, HAT-P-23 presents a mysterious problem with no definitive answers in the present but exciting novel opportunities in the future to study star-planet interactions. Therefore, we strongly recommend close monitoring of the HAT-P-23 system in the future.

2.2.10 WASP-114 b

WASP-114 b is a ~ 1.8 M_J planet in 1.5 day orbit around its star. It was recently discovered in 2016 by Barros et al. The one new transit observed at FLWO in r' filter is the only follow-up observation available so far. Table 2.6 summarizes the details of the observation along with the measured transit time.

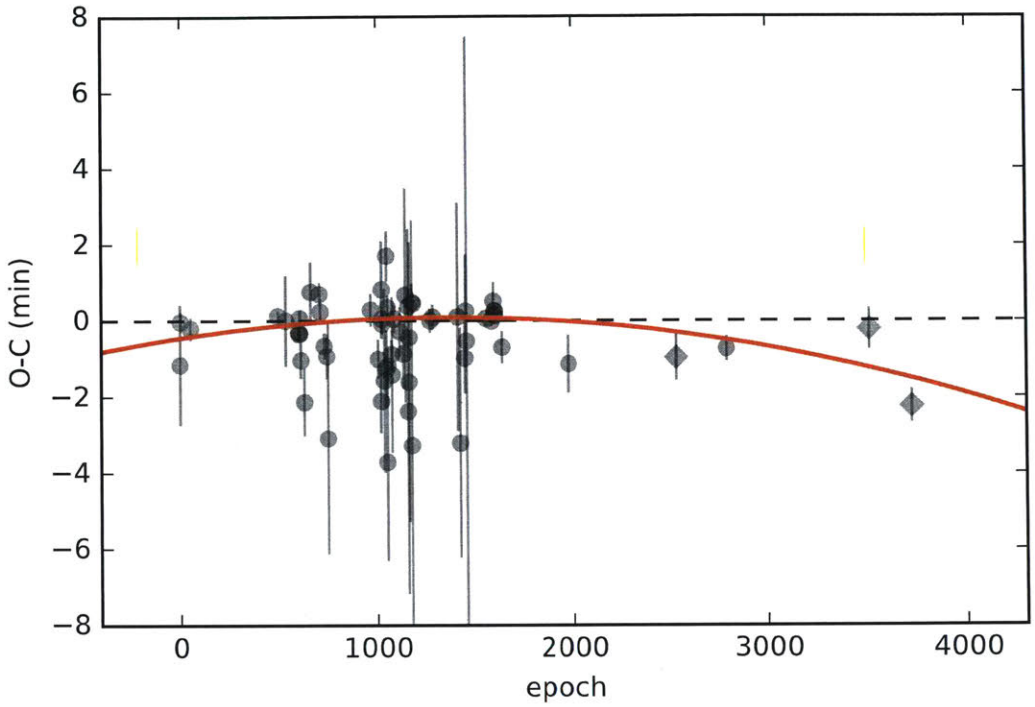

Figure 2-8: Timing residuals for WASP-19 b. The black circles are previously reported transit times and the black diamonds are new transit times obtained for this work.

Figures 2-11 and 2-12 show the light curve with its best-fit model and the timing residuals respectively. Currently we cannot draw any conclusions about the ephemeris of WASP-114 b because only two observation points are available. Future follow-up work is required.

2.2.11 WASP-122 b

WASP-122 b is a $\sim$ 1.4 M_J planet in 1.7 day orbit around its star. It was recently discovered in 2015 by Turner et al. Currently, we do not have any follow-up observations of WASP-122 b, though we are scheduled to carry out new observations from the LCO Telescope Network next season starting October 2018.

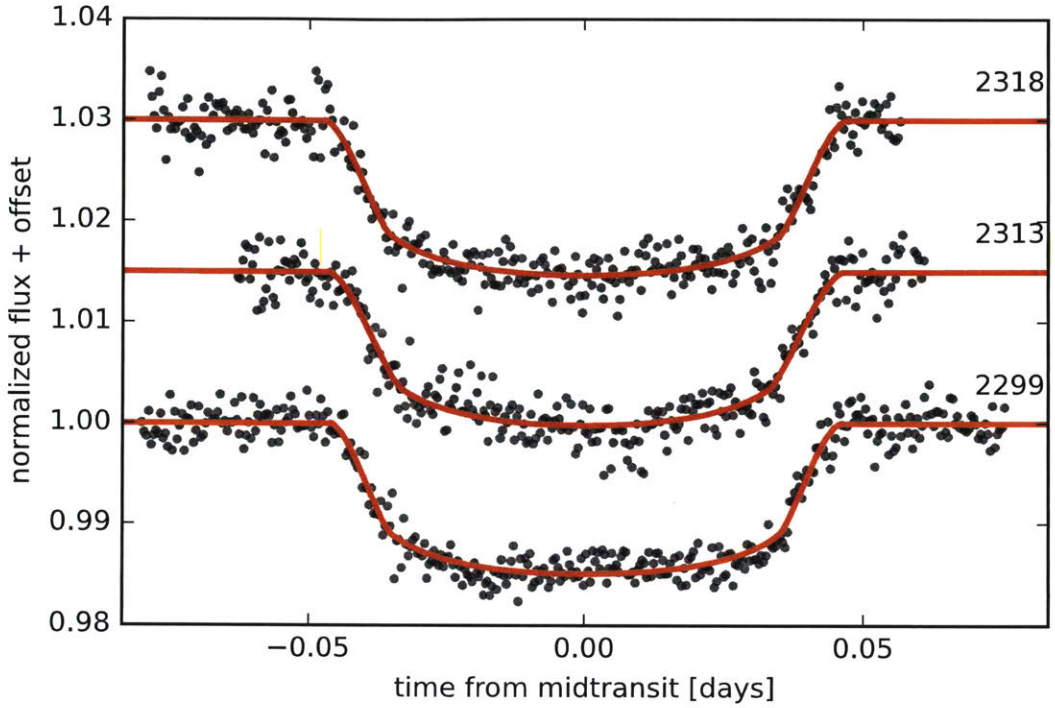

Figure 2-9: New transit light curves for HAT-P-23 b. Epoch numbers are printed to the right of each curve. Vertical offsets have been applied to separate the light curves.

2.2.12 WASP-72 b

WASP-72 b was discovered in 2013 by Gillon et al. using the TRAPPIST telescope at La Silla ESO Observatory (Chile). It is a ~ 1.5 M_J planet in 2.2 day orbit around its star. New data were obtained for WASP-72 b by Gillon et al. in $I+z$ filter using the same TRAPPIST telescope. Table 2.7 summarizes the observation details and the measured mid-transit times.

Figures 2-13 and 2-14 show the new light curves and timing residuals respectively. Since TRAPPIST is a relatively smaller telescope (60 cm diameter), the signal-to-noise ratio of the measured flux is low. As a result, the transit times are highly susceptible to spurious night-to-night variations. Furthermore, the timing precision is considerably worse than most other targets. Continued monitoring of WASP-72 is necessary in the future.

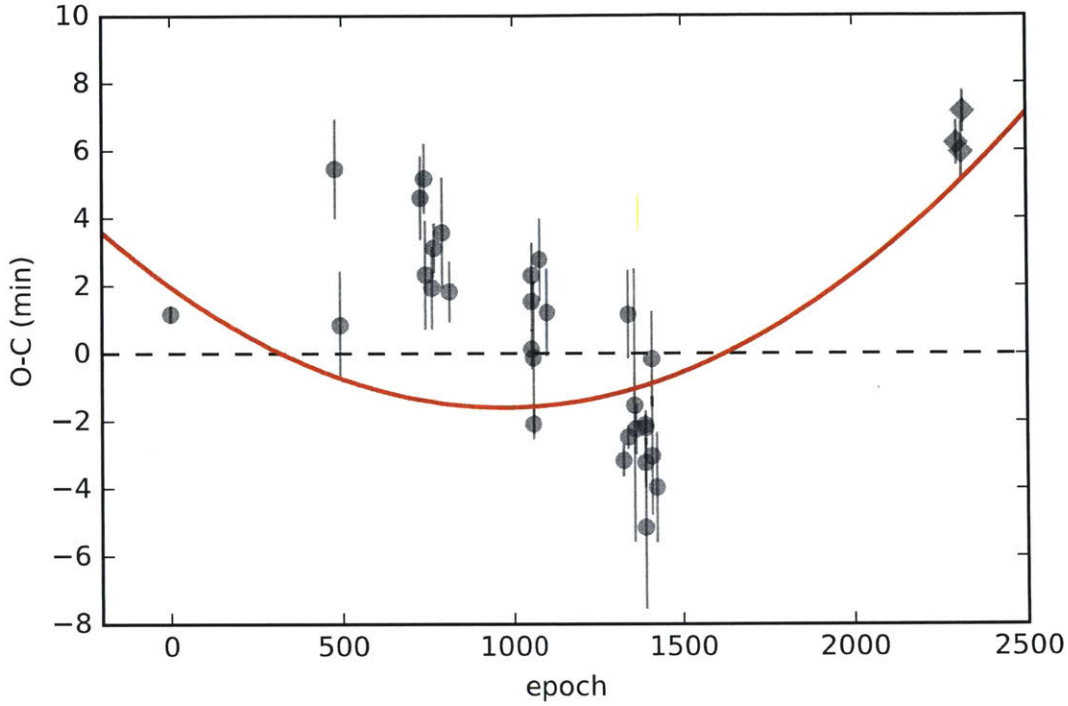

Figure 2-10: Timing residuals for HAT-P-23 b. The black circles are previously reported transit times and the black diamonds are new transit times obtained for this work. The red curve is the best-bit orbital decay model.

Target	Epoch	Date-Obs UTC	Exp (sec)	T_{mid} BJD_{TDB}	Unc (days)
WASP-114 b	882	2017 Oct 7	30	2458033.758338	0.00068

Table 2.6: Observation journal for WASP-114 b and calculated mid-transit times.

Target	Epoch	Date-Obs UTC	Exp (sec)	T_{mid} BJD_{TDB}	Unc (days)
WASP-72 b	937	2016 Sep 29	10	2457660.732737	0.00302
WASP-72 b	951	2016 Oct 30	10	2457691.773068	0.00248

Table 2.7: Observation journal for WASP-72 b and calculated mid-transit times.

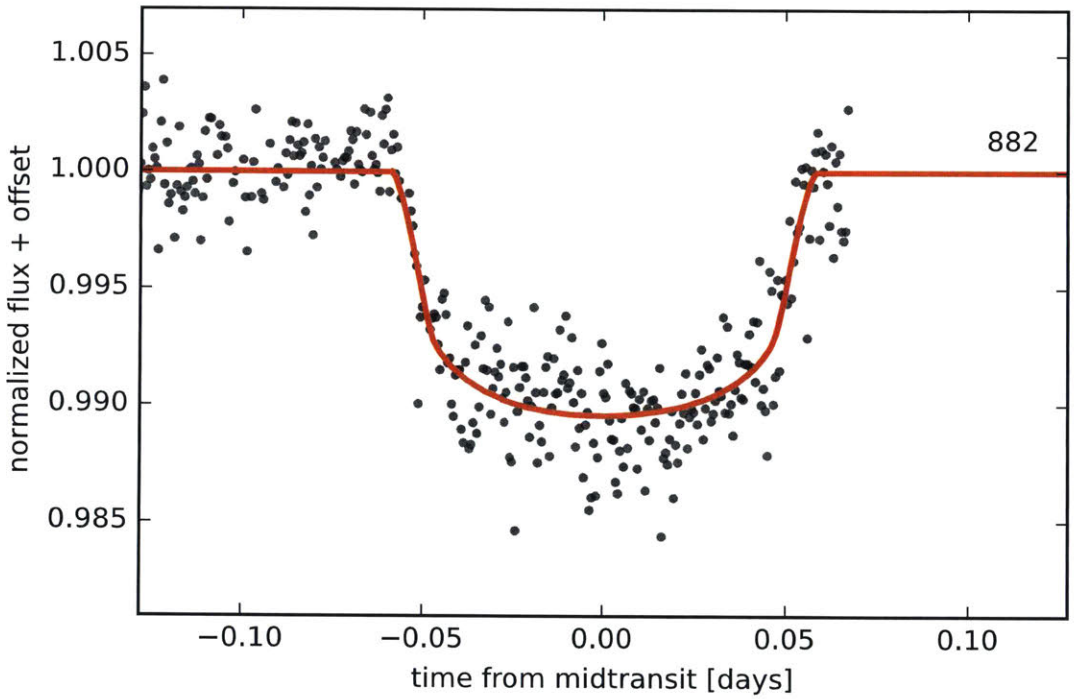

Figure 2-11: New transit light curve for WASP-114 b. Epoch number is printed on the right.

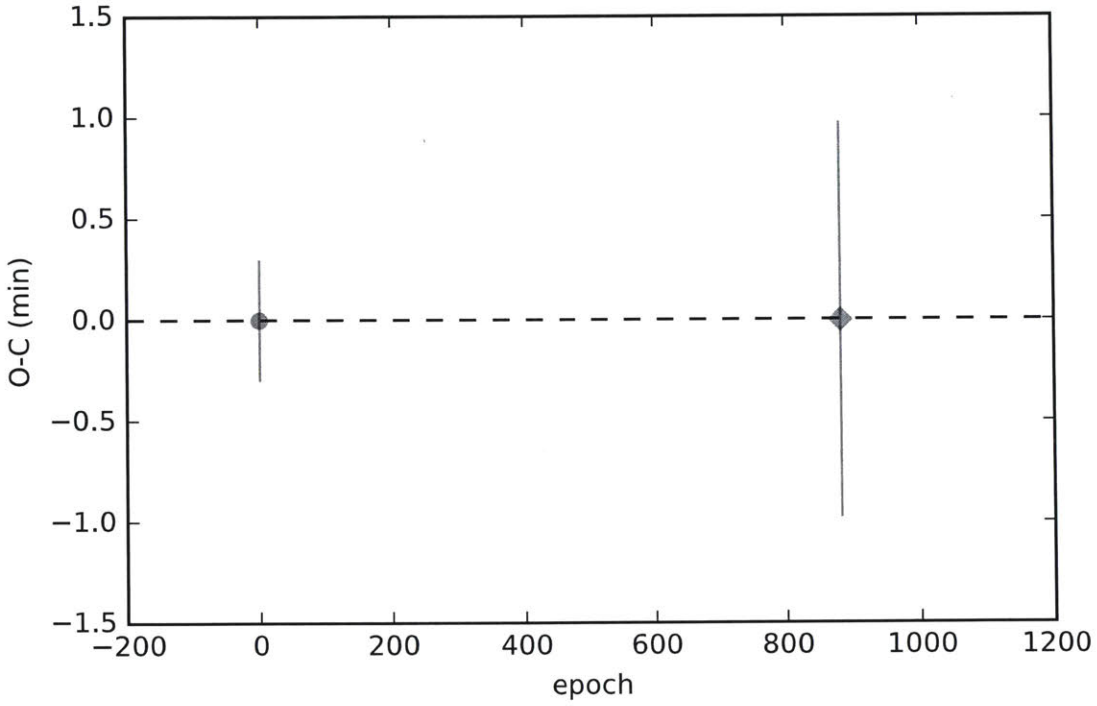

Figure 2-12: Timing residuals for WASP-114 b. The black circle is the discovery transit time and the black diamond is the new transit time obtained for this work.

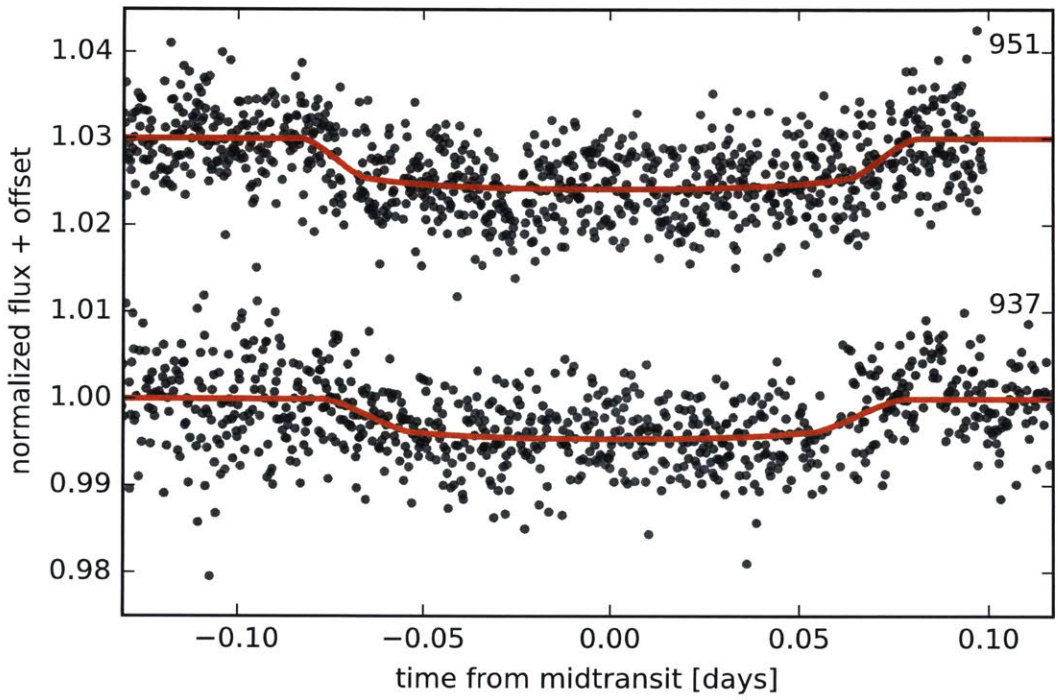

Figure 2-13: New transit light curves for WASP-72 b. Epoch numbers are printed to the right of each curve. Vertical offsets have been applied to separate the light curves.

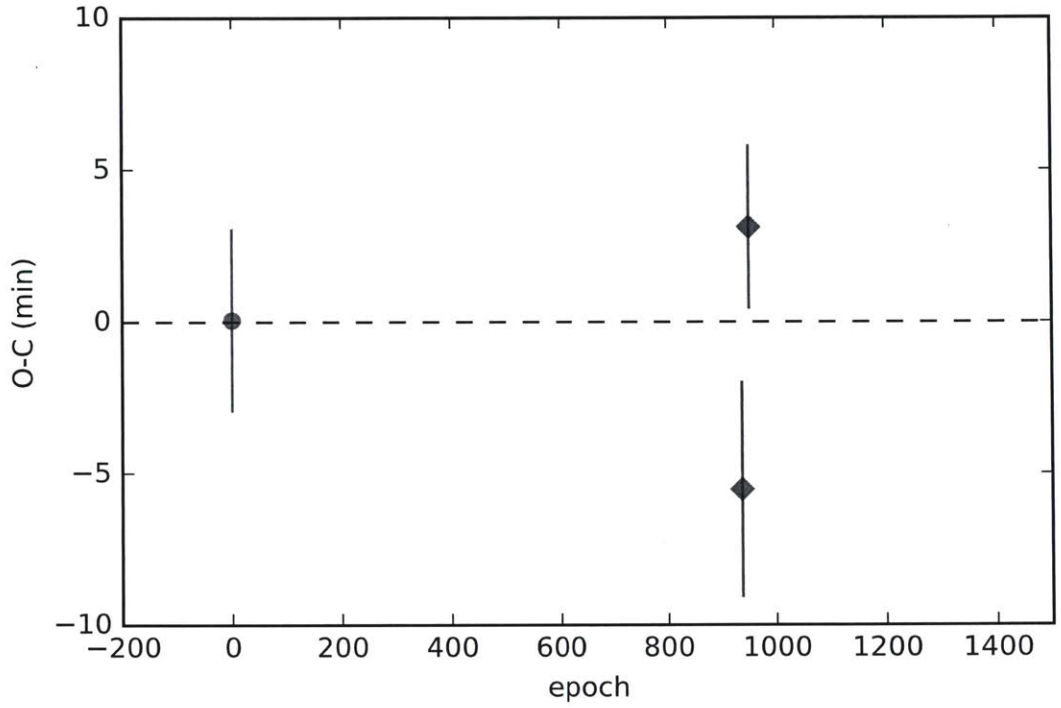

Figure 2-14: Timing residuals for WASP-72 b. The black circles are previously reported transit times and the black diamonds are new transit times obtained for this work.

Chapter 3

Apparently Decaying Orbit Of WASP-12 b

Note: This chapter discusses our results on the apparently decaying orbit of WASP-12 b. The contents of this chapter were published in The Astronomical Journal, 154:4 (10pp), 2017 July (© 2017. The American Astronomical Society. All rights reserved). This work was made possible by extensive inputs from Joshua Winn, Matthew Holman, Liang Yu, Drake Deming and Fei Dai, all of whom are listed as co-authors on the article.

Abstract

We present new transit and occultation times for the hot Jupiter WASP-12b. The data are compatible with a constant period derivative: $\dot{P} = -29 \pm 3$ ms yr^{-1} and $P/\dot{P} = 3.2$ Myr. However, it is difficult to tell whether we have observed orbital decay or a portion of a 14-year apsidal precession cycle. If interpreted as decay, the star's tidal quality parameter $Q_\star$ is about 2×10^5. If interpreted as precession, the planet's Love number is 0.44 ± 0.10. Orbital decay appears to be the more parsimonious model: it is favored by $\Delta\chi^2 = 5.5$ despite having two fewer free parameters than the precession model. The decay model implies that WASP-12 was discovered within the final $\sim$0.2% of its existence, which is an unlikely coincidence but harmonizes with independent evidence that the planet is nearing disruption. Precession does not invoke any temporal coincidence, but it does require some mechanism to maintain an eccentricity of $\approx$0.002 in the face of rapid tidal circularization. To distinguish unequivocally between decay and precession will probably require a few more years of monitoring. Particularly helpful will be occultation timing in 2019 and thereafter.

3.1 Introduction

More than 20 years have elapsed since the discovery of hot Jupiters (Mayor & Queloz 1995). The time may be ripe to confirm a long-standing theoretical prediction: the orbits of almost all of these planets should be shrinking due to tidal orbital decay (Rasio 1996, Sasselov 2003, Levrard 2009). This is because the star's rotational angular momentum is typically smaller than one-third of the orbital angular momentum, the critical value beneath which tidal evolution has no stable equilibrium (Hut 1980).

Tidal decay of hot Jupiters has been invoked to explain certain properties of the ensemble of star-planet systems. For example, the scarcity of gas giants with periods less than a day is suggestive of orbital decay (see, e.g. Jackson 2008, Hansen 2010, Penev 2012, Ogilvie 2014). The anomalously rapid rotation of some hot-Jupiter host stars has been attributed to transfer of the planet's orbital angular momentum (Penev 2016). The absence of hot Jupiters around subgiant stars may be caused by an acceleration of orbital decay when a star leaves the main sequence (Villaver & Livio 2009, Hansen 2010, Schlaufman & Winn 2013). Tidal decay might also be responsible for the lower occurrence of close-in planets around rapidly rotating stars (Teitler & Konigl 2014), or the realignment of stars and their planetary orbits (Matsakos & Konigl 2015). However, direct evidence for orbital decay has been lacking: there have been no clear demonstrations of a long-term period decrease due to orbital decay (see, e.g., Hoyer 2016, Wilkins 2017).

Another unfulfilled prediction is that the orbits of hot Jupiters should be apsidally precessing on a timescale of decades (Miralda-Escude 2002, Heyl & Gladman 2007, Pal & Kocsis 2008, Jordan & Bakos 2008), as long as the orbits are at least slightly eccentric. In particular, Ragozzine & Wolf (2009) noted that the theoretical precession rate is dominated by the contribution from the planet's tidally deformed mass distribution. They advocated a search for apsidal precession as a means of probing the interiors of hot Jupiters.

With an orbital period of 1.09 days, WASP-12b is one of the shortest-period giant planets known (Hebb 2009), and has been monitored for a decade. It is, therefore, an outstanding target in the search for orbital decay and apsidal precession. Maciejewski (2016) reported a decrease in the apparent period. Despite being the most convincing claim that has yet

been presented for orbital decay, those authors could not distinguish between true period shrinkage and a long-term oscillation of the apparent period due to apsidal precession. In this paper, we present new transit and occultation times (§ 3.2 and 3.3). We use all of the available data to test which model is favored by the data: a constant period derivative, or sinusoidal variations arising from apsidal precession (§ 3.4). We also discuss the implications of both models (§ 3.5) and prospects for future observations (§ 3.6).

3.2 New transit times

Between 2016 October and 2017 February, we observed seven transits of WASP-12 with the 1.2m telescope at the Fred Lawrence Whipple Observatory on Mt. Hopkins, Arizona. Images were obtained with the KeplerCam detector through a Sloan r'-band filter. The typical exposure time was 15 s, chosen to give a signal-to-noise ratio of about 200 for WASP-12. The raw images were processed by performing standard overscan correction, debiasing, and flat-fielding with IRAF[1]. Aperture photometry was performed for WASP-12 and an ensemble of 7-9 comparison stars of similar brightness. The aperture radius was chosen to give the smallest scatter in the flux outside of the transits, and was generally 7-8 pixels. The reference signal was generated by summing the flux of the comparison stars. The flux of WASP-12 was then divided by this reference signal to produce a time series of relative flux. Each time series was normalized to have unit flux outside of the transit. The time stamps were placed on the $\mathrm{BJD_{TDB}}$ system using the code of Eastman (2010).

We fitted a Mandel & Agol 2002 model to the data from each transit. The parameters of the transit model were the midtransit time, the planet-to-star radius ratio ($R_\mathrm{p}/R_\star$), the scaled stellar radius ($R_\star/a$), and the impact parameter ($b = a\cos i/R_\star$). For given values of $R_\star/a$ and b, the transit timescale is proportional to the orbital period [see, e.g., Eqn. (19) of Winn (2010). To set this timescale, we held the period fixed at 1.09142 days, although the individual transits were fitted separately with no requirement for periodicity. To correct for differential extinction, we allowed the apparent magnitude to be a linear function of airmass,

[1]The Image Reduction and Analysis Facility (IRAF) is distributed by the National Optical Astronomy Observatory, which is operated by the Association of Universities for Research in Astronomy (AURA) under a cooperative agreement with the National Science Foundation.

giving two additional parameters. The limb darkening law was assumed to be quadratic, with coefficients held fixed at the values ($u_1 = 0.32$, $u_2 = 0.32$) tabulated by Claret & Bloemen (2011) for a star with the spectroscopic parameters given by Hebb (2009).[2]

To determine the credible intervals for the parameters, we used the *emcee* Markov Chain Monte Carlo (MCMC) code written by Foreman-Mackey (2013). The transition distribution was proportional to $\exp(-\chi^2/2)$ with

$$\chi^2 = \sum_{i=1}^{N} \left(\frac{f_{\mathrm{obs},i} - f_{\mathrm{calc},i}}{\sigma_i} \right)^2 , \tag{3.1}$$

where $f_{\mathrm{obs},i}$ is the observed flux at time t_i and $f_{\mathrm{calc},i}$ is the corresponding flux of the model. The uncertainties σ_i were set equal to the standard deviation of the out-of-transit data. In a few cases, the pre-ingress scatter was noticeably different than the post-egress scatter; for those observations, we assigned σ_i by linear interpolation between the pre-ingress and post-egress values.

Figure 3-1 shows the light curves and the best-fit models. Table 1 reports the midtransit times and their uncertainties. For convenience, this table also includes the new occultation times described below, as well as the previously reported times that are analyzed in Section 3.4. The results for the other transit parameters were consistent with the previous results of Maciejewski (2013), with larger uncertainties.

Time-correlated noise is evident in some of the new light curves. Although we made no special allowance for these correlations in our analysis, we have reason to believe that the quoted uncertainties are reliable. When these seven new midtransit times are fitted with a linear function of epoch, we obtain $\chi^2_{\mathrm{min}} = 5.1$ with five degrees of freedom. When the period is held fixed at the value derived from all 10 years of timing data, we obtain $\chi^2_{\mathrm{min}} = 7.8$ with six degrees of freedom. These tests suggest that the uncertainties are not substantially underestimated. Furthermore, spurious timing variations would be random from night to night, whereas our long-term timing analysis (Section 3.4) reveals that all seven new midtransit times produce residuals of the same sign and amplitude.

[2]For this purpose we used the online code of Eastman (2013): http://astroutils.astronomy.ohio-state.edu/exofast/limbdark.shtml

3.3 New occultation times

We measured two new occultation times based on hitherto unpublished *Spitzer* observations in 2013 December (program 90186, P.I. Todorov). Two different transits were observed, one at 3.6 μm and one at 4.5 μm. The data take the form of a time series of 32x32-pixel subarray images, with an exposure time of 2.0 s per image. The data were acquired over a wide range of orbital phases, but for our purpose, we analyzed only the $\approx$14,000 images within 4 hours of each occultation. We also reanalyzed the *Spitzer* occultation presented by Deming (2015) using the technique described below.

We determined the background level in each image by fitting a Gaussian function to the histogram of pixel values, after excluding the high flux values associated with the star. The centroid of the fitted Gaussian function was taken to be the background value and was subtracted from each image prior to performing aperture photometry.

We used two different schemes to choose photometric aperture sizes. In the first scheme, we used 11 apertures ranging in radius from 1.6-3.5 pixels in average increments of 0.2 pixel. In the second scheme, we tried 11 apertures for which the radius was allowed to vary at each time step, based on the procedure described in Appendix A of Lewis (2013). In this procedure, the aperture radius is taken to be the sum of a constant (ranging from 0-2 pixels) and the noise pixel radius, defined as the square root of the ratio of the square of the total flux integrated over all pixels divided by the sum of the squared-fluxes in individual pixels. The noise pixel radius is specific to each image and allows for possible changes in the shape of the pixel response function with position. We also tried two different methods to choose the center of the apertures: fitting a two-dimensional Gaussian function to the stellar image, and computing the flux-weighted center-of-light. Hence, there were four versions of the photometry: constant versus variable aperture radii, and Gaussian centroiding versus center-of-light. Each of those four versions contains 11 time series with different aperture sizes.

We corrected for the well-known intrapixel sensitivity variations using pixel-level decorrelation [PLD; (Deming 2015)]. In PLD, the flux time series is modeled as the sum of the astrophysical variation, a temporal baseline, and a weighted sum of the (normalized) time

series of each pixel comprising the point-spread function. Because each pixel value is divided by the total brightness of the star in that image, PLD effectively separates astrophysical information and *Spitzer* detector effects. PLD has also been used to produce high-quality photometry from *K2* data (Luger 2016).

Our implementation of PLD operates on time-binned data [see Sec. 3.1 of (Deming 2015)]. Over a trial range of occultation midpoints and median aperture radii, the code uses linear regression to find the best-fit occultation depth and pixel coefficients. We provisionally adopt the midpoint that produces the best fit (smallest χ^2). The code then varies the aperture radius from among the 11 possible values and the duration of the time bins. The optimal values of the radius and bin size are determined by examining the (Allan 1966) deviation relation of the residuals and identifying the case that comes closest to the ideal relation.[3] Then, an MCMC procedure is used to optimize the light-curve parameters (including the time of mid-occultation), pixel coefficients, and temporal baseline coefficients. The temporal baseline was taken to be a quadratic function of time, which was sufficient to describe the phase-curve variation in the vicinity of the occultation.

After performing these steps for all four different versions of the photometry, we adopted the version that came closest to achieving the theoretical photon noise limit. For the 3.6 μm data, the adopted version used 10-frame binning, center-of-light centroiding, and a constant aperture radius of 2.3 pixels. For the 4.5 μm data, the adopted version used 10-frame binning, center-of-light centroiding, and a constant aperture radius of 2.2 pixels. With these choices, we achieved a noise level of 1.29 and 1.24 times the theoretical photon noise limit at 3.6 and 4.5 μm, respectively. The uncertainty in the midpoint of each occultation was determined from the standard deviation of the (very nearly Gaussian) marginalized posterior distribution. The new light curves are shown in Figure 3-2, and the times are given in Table 1. The best-fit central times are relatively insensitive to the version of the photometry adopted in the final solution. The very worst of the four photometry solutions for the 3.6 and 4.5 μm data gave midpoints differing by 31 and 75 seconds (0.3σ and 0.6σ), respectively.

[3]The Allan deviation relation expresses how the standard deviation of the binned residuals varies with bin size. For ideal white noise, it should decrease as the inverse square root of the bin size.

3.4 Timing analysis

We included all of the data we could find in the literature for which (i) the analysis was based on observations of a single event, (ii) the midpoint was allowed to be a completely free parameter, and (iii) the time system is documented clearly. The tabulated occultation times have not been corrected for the light-travel time across the diameter of the orbit. For the timing analysis described below, the occultation times were corrected by subtracting $2a/c = 22.9$ s.

We fitted three models to the timing data using the MCMC method. The first model assumes a circular orbit and a constant orbital period:

$$t_{\rm tra}(E) = t_0 + PE, \tag{3.2}$$

$$t_{\rm occ}(E) = t_0 + \frac{P}{2} + PE, \tag{3.3}$$

where E is the epoch number. Figure 3-3 displays the residuals with respect to this model. The fit is poor, with $\chi^2_{\rm min} = 197.6$ and 111 degrees of freedom. The transit residuals follow a negative parabolic trend, indicating a negative period derivative. Our new data—the square points at the rightmost extreme of the plot—follow the trend that had been established by Maciejewski (2016). Thus, we confirm the finding of (Maciejewski 2016) that the transit interval is slowly shrinking.

Next we fitted a model that assumes a circular orbit and a constant period derivative:

$$t_{\rm tra}(E) = t_0 + PE + \frac{1}{2}\frac{dP}{dE}E^2, \tag{3.4}$$

$$t_{\rm occ}(E) = t_0 + \frac{P}{2} + PE + \frac{1}{2}\frac{dP}{dE}E^2. \tag{3.5}$$

The red curves in Figure 3-3 shows the best fit, which has $\chi^2_{\rm min} = 118.5$ and 110 degrees of freedom. Both the transit and occultation data are compatible with the model. The implied period derivative is

$$\frac{dP}{dt} = \frac{1}{P}\frac{dP}{dE} = -(9.3 \pm 1.1) \times 10^{-10} = -29 \pm 3 \text{ ms yr}^{-1}. \tag{3.6}$$

In the third model, the orbit is slightly eccentric and undergoing apsidal precession:

$$t_{\rm tra}(E) = t_0 + P_{\rm s}E - \frac{eP_{\rm a}}{\pi}\cos\omega, \tag{3.7}$$

$$t_{\rm occ}(E) = t_0 + \frac{P_{\rm a}}{2} + P_{\rm s}E + \frac{eP_{\rm a}}{\pi}\cos\omega, \tag{3.8}$$

where e is the eccentricity, ω is the argument of pericenter, $P_{\rm a}$ is the anomalistic period and $P_{\rm s}$ is the sidereal period. The argument of pericenter advances uniformly in time,

$$\omega(E) = \omega_0 + \frac{d\omega}{dE}E, \tag{3.9}$$

and the two periods are related by

$$P_{\rm s} = P_{\rm a}\left(1 - \frac{d\omega/dE}{2\pi}\right). \tag{3.10}$$

These expressions are based on Eqn. (15) of (Gimenez & Bastero1995), in the limit of low eccentricity and high inclination. This model has 5 parameters: t_0, $P_{\rm s}$, e, ω_0, and $d\omega/dE$.

The blue curves in Figure 3-3 show the best-fit precession model. The main difference between the decay and precession models is that apsidal precession produces anticorrelated transit and occultation timing deviations, while the orbital decay model produces deviations of the same sign. The precession fit has $\chi^2_{\rm min} = 124.0$ and 108 degrees of freedom. The model achieves a reasonable fit by adjusting the precession period to be longer than the observing interval. In this way, the parabolic trend can be matched by the downward-curving portion of a sinusoidal function. However, there is tension between the need for enough downward curvature in the transit deviations to fit the earliest data and a small enough upward curvature in the occultation deviations to fit the most recent data.

The orbital decay model provides the best fit. It is better than the precession model by $\Delta\chi^2 = 5.5$, despite the handicap of having two fewer free parameters. The Akaike Information Criterion (AIC) and Bayesian Information Criterion (BIC) are widely used statistics to

choose the most parsimonious model that fits the data:

$$\alpha = \mathrm{AIC} = \chi^2 + 2k, \tag{3.11}$$

$$\beta = \mathrm{BIC} = \chi^2 + k \log n, \tag{3.12}$$

where n is the number of data points and k is the number of free parameters. In this case, $n = 113$, $k = 3$ for decay, and $k = 5$ for precession. The AIC favors the decay model by $\Delta\alpha = 9.46$, corresponding to a likelihood ratio of $\exp(\Delta\alpha/2) = 113$. The BIC favors the orbital decay model by $\Delta\beta = 14.91$, corresponding to an approximate Bayes factor of $\exp(\Delta\beta/2) = 1730$.

Table 3.1 gives the best-fit parameters for all three models. In summary, a constant period has been firmly ruled out, and orbital decay is statistically favored over apsidal precession as the best explanation for the timing data. However, the statistical significance of the preference for orbital decay is modest and depends on the reliability of the quoted uncertainties for all of the timing data, which come from different investigators using different methods. For example, when the earliest data point is omitted, orbital decay is still preferred but $\Delta\chi^2$ is reduced to 2.0. For these reasons, and out of general caution, we do not regard apsidal precession as being definitively ruled out. Further observations are needed.

3.5 Implications

3.5.1 Orbital decay

To explore the implications of the best-fit models, we assume, for the moment, that the orbital decay interpretation is correct. Based on the current decay rate, the period would shrink to zero in

$$\frac{P}{dP/dt} = 3.2 \text{ Myr}. \tag{3.13}$$

The future lifetime of the planet is likely to be even shorter, because the decay rate is expected to increase rapidly with decreasing period.

In the simplified "constant phase lag" model for tidal evolution, the period derivative is

$$\frac{dP}{dt} = -\frac{27\pi}{2Q_\star}\left(\frac{M_\mathrm{p}}{M_\star}\right)\left(\frac{R_\star}{a}\right)^5, \tag{3.14}$$

which we obtained by applying Kepler's third law to Eqn. (20) of Goldreich & Soter (1966). Here, $Q_\star$ is the "modified quality factor" of the star's tidal oscillations (often designated elsewhere as $Q'_\star$). For the case of WASP-12, $M_\mathrm{p}/M_\star = 9.9 \times 10^{-4}$ and $a/R_\star = 3.097$ (Chan 2011), giving

$$Q_\star \approx 2 \times 10^5. \tag{3.15}$$

This value for $Q_\star$ is smaller than the typical range of 10^{6-7} that has been inferred through ensemble analyses of binary stars and star-planet systems (see, e.g. Meibom & Mathieu 2005,Hansen 2010,Penev 2012). One exception is Jackson (2008), who found $Q_\star \sim 10^{5.5}$ based on the period-eccentricity distribution of hot Jupiters. This is consistent with our result.

Theoretically, the quality factor should depend on the orbital period, perturbation strength, and internal structure of the star (Ogilvie 2014). Recently, (Essick & Weinberg 2016) calculated $Q_\star$ for hot Jupiters perturbing solar-type stars, based on the nonlinear interactions and dissipation of tidally driven g-modes. For the mass ratio and period of WASP-12, their Eqn. (26) predicts $Q_\star = 4 \times 10^5$, close to the observed value. However, their calculation pertained to stars with a radiative core and a convective envelope, and it is not clear that WASP-12 belongs in this category. With $T_\mathrm{eff} = 6100$ K (Torres 2012), WASP-12 is right on the borderline between stars with convective and radiative envelopes. In fact, we wonder if this coincidence—lying right on the Kraft break—could be related to the apparently rapid dissipation rate. The star may have a convective core and a convective envelope, separated by a radiative zone, perhaps leading to novel mechanisms for wave dissipation.

3.5.2 Apsidal precession

Assuming instead that the apsidal precession model is correct, the orbital eccentricity is 0.0021 ± 0.0005. This is compatible with the upper limit of 0.05 from observations of the

spectroscopic orbit (Husnoo 2012). The observed precession rate is $\dot{\omega} = 26 \pm 3$ deg yr^{-1}, corresponding to a precession period of 14 ± 2 years.

(Ragozzine & Wolf 2009) showed that for systems resembling WASP-12, the largest contribution to the theoretical apsidal precession rate is from the planet's tidal deformation. The rate is proportional to the planet's Love number $k_{\rm p}$, a dimensionless measure of the degree of central concentration of the planet's density distribution. Lower values of $k_{\rm p}$ correspond to more centrally concentrated distributions, which are closer to the point-mass approximation and, therefore, produce slower precession. Eqn. (14) of Ragozzine & Wolf (2009) can be rewritten for this case as

$$\frac{d\omega}{dE} = 15\pi k_{\rm p} \left(\frac{M_\star}{M_{\rm p}}\right) \left(\frac{R_{\rm p}}{a}\right)^5 . \tag{3.16}$$

Using the measured precession rate and relevant parameters of WASP-12, this equation gives $k_{\rm p} = 0.44 \pm 0.10$. If this interpretation is confirmed, it would be a unique constraint on an exoplanet's interior structure, in addition to the usual measurements of mass, radius, and mean density. For Jupiter, a value of $k_{\rm p} = 0.59$ has been inferred from its observed gravity moments (Wahl 2016). Therefore the precession interpretation for WASP-12b suggests that its density distribution has a similar degree of central concentration as Jupiter, and perhaps somewhat higher.

3.5.3 Prior probabilities

It is worth contemplating the "prior probability" of each model. By this, we mean the chance that the circumstances required by each model would actually occur, independently of the goodness-of-fit to the data. At face value, both models imply that we are observing WASP-12 at a special time, in violation of the "temporal Copernican principle" articulated by Gott (1993). It is difficult, however, to decide which model requires the greater coincidence.

Given the star's main-sequence age of 1700 ± 800 Myr Chan (2011), the orbital decay model would have us believe we are witnessing the last $\sim$0.2% of the planet's life. If we observed a single system at a random time, this would require a one-in-500 coincidence. However, WASP-12 is not the only hot Jupiter that we and others have been monitoring.

There are about 10 other good candidates with comparably low $a/R_\star$, increasing the odds of the coincidence by an order of magnitude.

It is noteworthy that other investigators have argued on independent grounds that WASP-12b is close to death. Fossati (2010), Haswell (2012), and Nichols (2015) have presented near-ultraviolet transit spectroscopy consistent with an extended and escaping exosphere. The resulting mass loss process has been studied theoretically by Li (2010), Lai (2010), and Bisikalo (2013). Most recently, Jackson (2017) developed a new theory for Roche lobe overflow and identified WASP-12 as a likely case of rapid mass loss.

It is also possible that orbital decay occurs in fits and starts, because of strong and erratic variations in the dissipation rate with the forcing period [see, e.g., Ogilvie & Lin 2007, Barker & Ogilvie 2010]. Thus, the planet may be experiencing a brief interval of rapid decay. This does not eliminate the requirement for a coincidence, because one would expect to discover the system in one of the more prolonged states of slow dissipation. However, it does mean that the planet's future lifetime may be longer than the current value of $P/\dot{P}$.

As for apsidal precession, the trouble is the very short expected timescale for tidal orbital circularization. This process is thought to be dominated by dissipation within the planet, rather than the star. Eqn. (25) of Goldreich & Soter (1966), relevant to this case, can be rewritten

$$\tau_e = \frac{e}{|de/dt|} = \frac{2Q_\mathrm{p}}{63\pi}\left(\frac{M_\mathrm{p}}{M_\star}\right)\left(\frac{a}{R_\mathrm{p}}\right)^5 P_\mathrm{orb}. \tag{3.17}$$

For WASP-12, this gives $\tau_e \sim 0.5$ Myr, assuming $Q_\mathrm{p} \sim 10^6$. At this rate, even 4 Myr of tidal evolution would reduce the eccentricity below 10^{-3}. Of course, the planetary quality factor Q_p could be larger than the standard value of 10^6, or the tidal model leading to the preceding equation could be a gross misrepresentation of the actual circularization process.

There may also be some process that continually excites the eccentricity. One possibility is gravitational forcing by another planet, although no other nearby planets are known in the WASP-12 system (Knutson 2014). An intriguing possibility is eccentricity excitation by the gravitational perturbations from the star's convective eddies. In this scenario, proposed by Phinney (1992) to explain the small but nonzero eccentricities of pulsars orbiting white dwarfs, the system reaches a state of equipartition between the energy of eccentricity oscil-

lations (epicyclic motion) and the kinetic energy of turbulent convection. To our knowledge, this theory has only been developed for post-main-sequence stars [see, e.g. Verbunt & Phinney 1995, Rafikov 2016]. It is not obvious that this theory would apply to WASP-12 and be compatible with $e \sim 10^{-3}$.

Should further theoretical investigations reveal that this mechanism (or any other) could naturally maintain the orbital eccentricity at the level of 10^{-3}, then the apsidal precession model would require no special coincidence. Neither would it require unique circumstances; it is possible that eccentricities of this order could exist in other hot Jupiter systems and have remained undetected. Thus, the identification of a natural eccentricity-excitation mechanism would swing the prior-probability balance in the direction of apsidal precession.

3.5.4 Other possible explanations

To this point, we have presented orbital decay and apsidal precession as the only possible reasons for an apparent period decrease. Another possibility is that the star is accelerating toward Earth, due to the force from stellar companions or wide-orbiting planets. This would produce a negative apparent period derivative of $\dot{v}_{\rm r}P/c$, where $v_{\rm r}$ is the radial velocity. Based on long-term Doppler monitoring, Knutson (2014) placed an upper limit for WASP-12 of $|\dot{v}_{\rm r}| < 0.019$ m s^{-1} day^{-1} (2σ), which, in turn, limits the apparent $\dot{P}$ to be smaller than 7×10^{-11}. This is an order of magnitude too small to be responsible for the observed period derivative. Of course, none of these phenomena are mutually exclusive. The system may be experiencing a combination of orbital decay, apsidal precession, and radial acceleration, although joint modeling of these effects is not productive with the current data.

Rafikov (2009) described two other phenomena that cause changes in the apparent period of a transiting planet. The first is the Shklovskii effect, wherein the star's proper motion leads to a changing radial velocity and a nonzero second derivative of the light-travel time. This is already ruled out by Doppler observations of the radial acceleration. For completeness, though, we note that the observed distance d and proper motion μ imply a period derivative of $P\mu^2 d/c \sim 6 \times 10^{-15}$, too small to explain the data. The second phenomenon, also dependent on proper motion, is the apparent apsidal precession caused by our changing viewing angle. The resulting period derivative is of order $\sim(P\mu)^2/2\pi$, which in this case is $\sim 10^{-21}$, too

small by many orders of magnitude.

3.6 Future prospects

With WASP-12, we are fortunate that both possibilities—orbital decay and apsidal precession—lead to interesting outcomes. It will soon be possible to measure the tidal dissipation rate of a star, or the tidal deformability of an exoplanet, either of which would be a unique achievement. To help understand the requirements for a definitive verdict, Figure 3-4 shows the future projections of a sample of 100 models that provide satisfactory fits to the data, drawn randomly from our converged Markov chains.

For the transits, the two families of models become separated by a few minutes by 2021-22. The occultation models diverge earlier, and are separated by a few minutes in 2019-20. Thus, while continued transit timing is important, the most rapid resolution would probably come from observing occultations a few years from now. In principle, transit duration variations (TDV) would also help to distinguish between the two models, but the expected amplitude is (Pal & Kocsis 2008)

$$\mathrm{TDV} \sim \frac{P}{2\pi}\left(\frac{R_\star}{a}\right) e\cos\omega \sim 10 \text{ sec}, \tag{3.18}$$

which will be difficult to detect.

In this paper, we have focused on the timing anomalies of WASP-12. This system has other remarkable features we have not even discussed. The star's equator is likely to be misaligned with the orbital plane (Schlaufman 2010, Albrecht 2012). The star is also part of a hierarchical three-body system, with a tight pair of M dwarfs orbiting the planet-hosting star at a distance of about 265 AU (Bechter 2014). Detailed modeling of the star's interior structure and and tidal evolution is warranted, as are continued observations of transits and occultations.

Parameter	Value (unc)
Constant period	
Reference epoch, t_0 [$\mathrm{BJD_{TBD}}$]	2456305.455609(28)
Period, P [days]	1.091420025(47)
Orbital decay	
Reference epoch, t_0 [$\mathrm{BJD_{TBD}}$]	2456305.455790(35)
Period at reference epoch, P [days]	1.091420078(47)
dP/dE [days]	$-1.02(11) \times 10^{-9}$
Apsidal precession	
Reference epoch, t_0 [$\mathrm{BJD_{TBD}}$]	2456305.45509(15)
Sidereal period, P_{sid} [days]	1.09141993(15)
Eccentricity, e	0.00208(47)
A.O.P. at reference epoch, ω_0 [rad]	2.92(19)
Precession rate, $d\omega/dE$ [rad epoch^{-1}]	0.00133(18)

Table 3.1: Best-fit model parameters

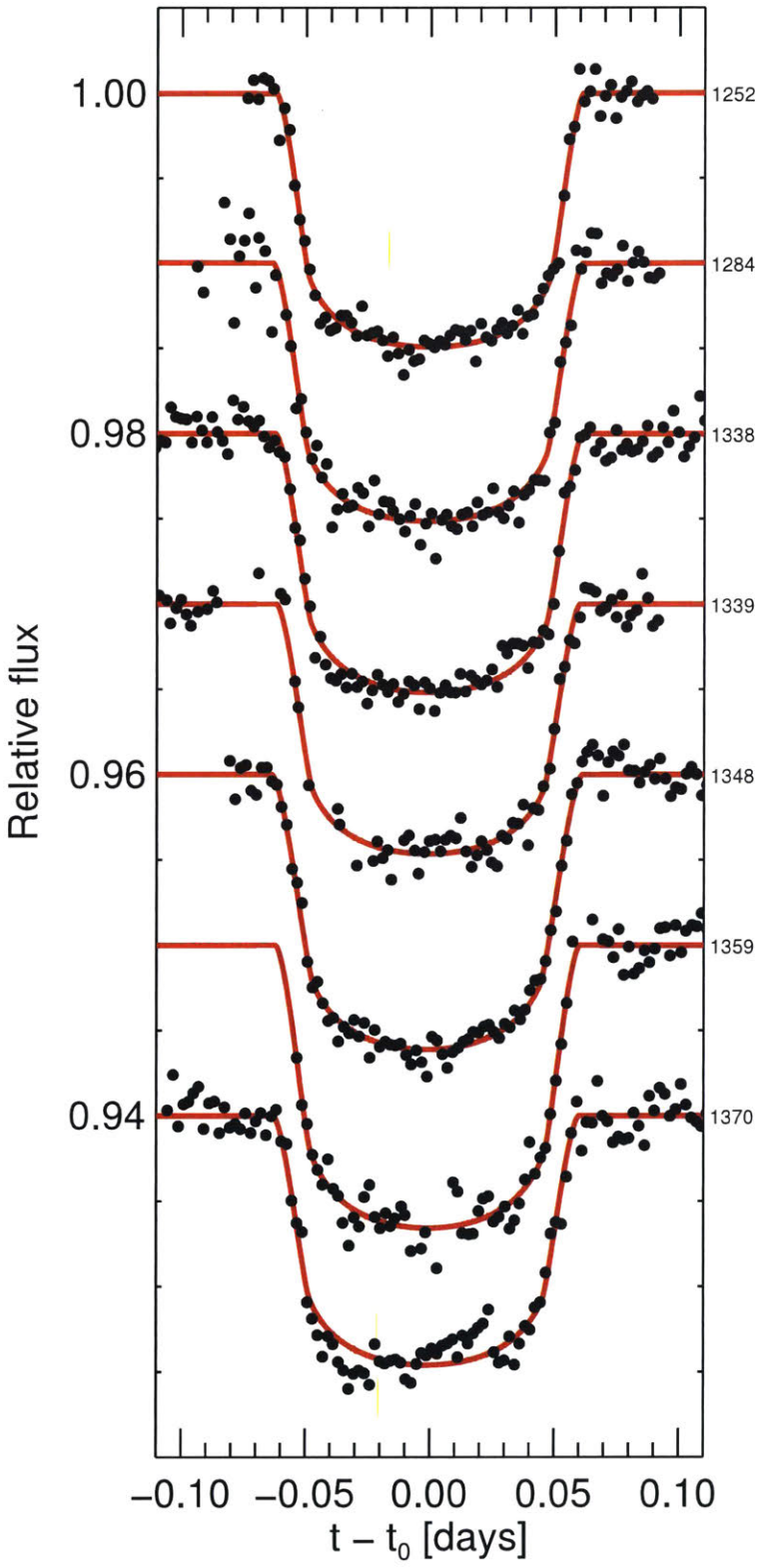

Figure 3-1: **New transit light curves.** Black points are based on observations with the FLWO 1.2m telescope in the Sloan r' band. Red curves are the best-fit models. Epoch numbers are printed to the right of each curve. Vertical offsets have been applied to separate the light curves.

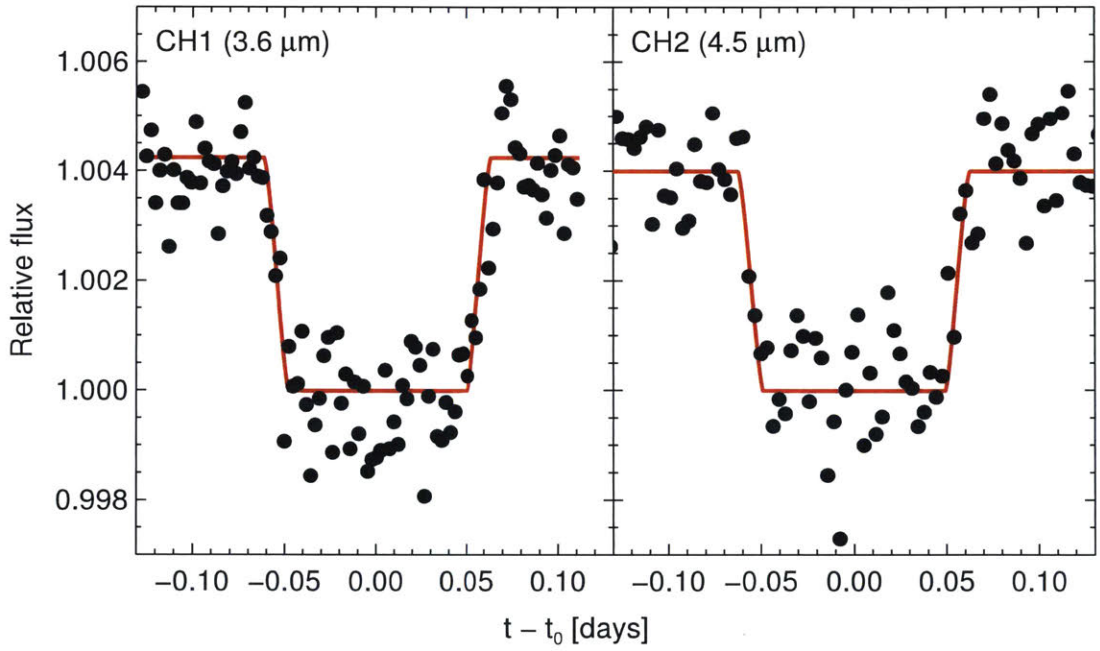

Figure 3-2: **New occultation light curves.** Black points are the binned *Spitzer* measurements from epochs 305 (left) and 308 (right). Red curves are the best-fit models.

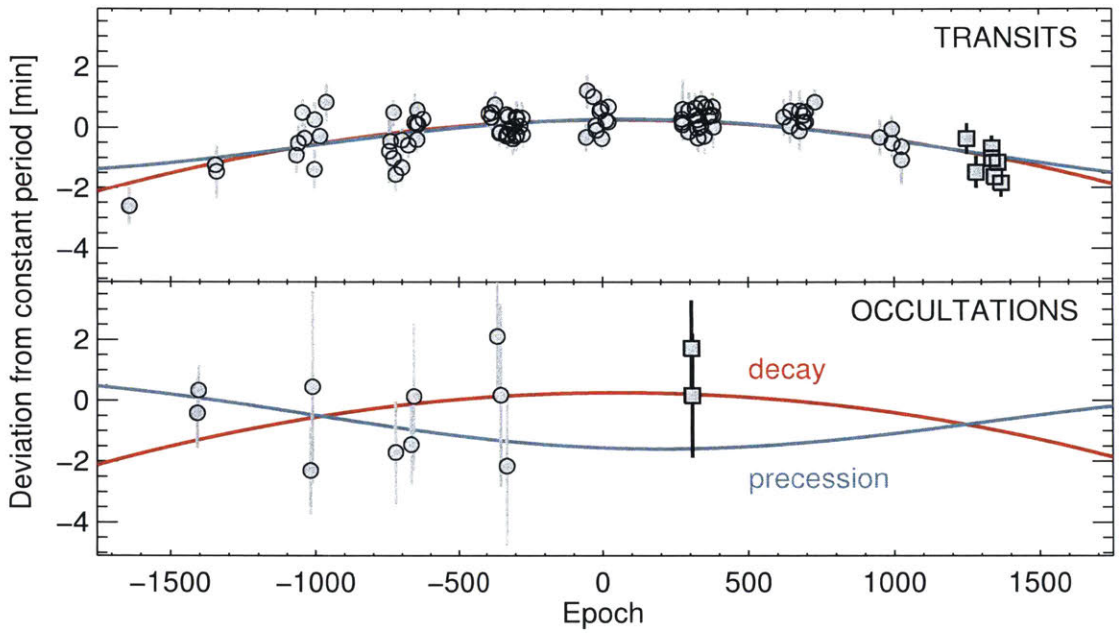

Figure 3-3: **Timing residuals for WASP-12.** Each data point is the difference between an observed eclipse time and the prediction of the best-fit constant-period model. The top panel shows transit data and the bottom panel shows occultation data. Circles are previously reported data, and squares are new data. The blue curves show the best-fit precession model, for which transit and occultation deviations are anticorrelated. The red curves show the best-fit orbital decay model, in which the transit and occultation deviations are the same.

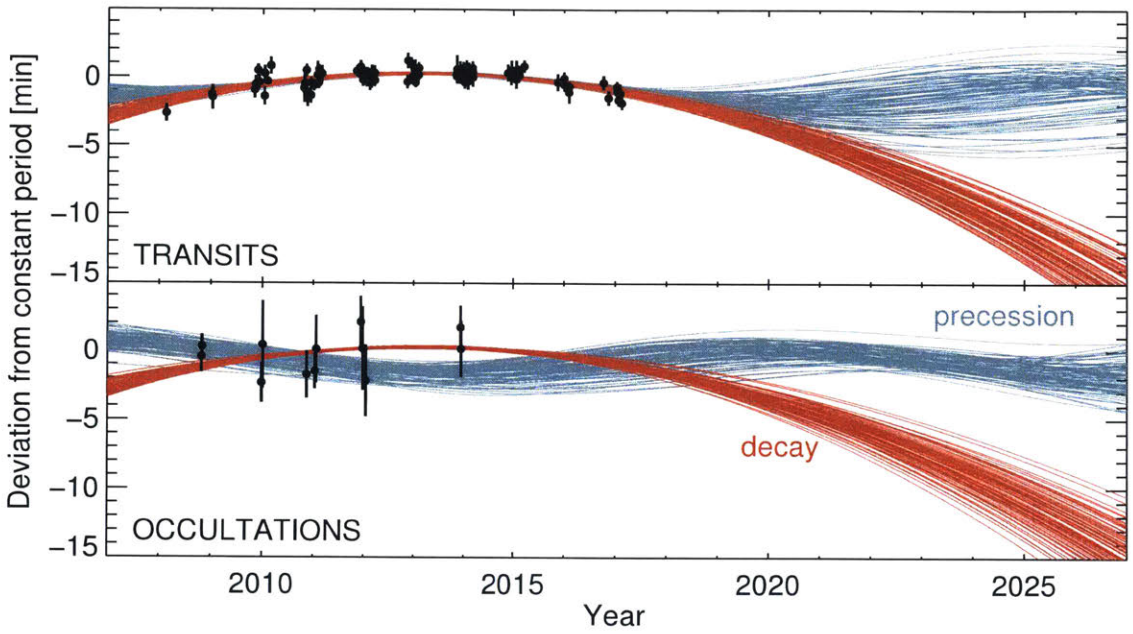

Figure 3-4: **Possible futures for WASP-12.** For each of the two models, we randomly drew 100 parameter sets from our Markov chains. Shown here are the extrapolations of those models to future times.

Chapter 4

Alternative Explanations For Ephemeris of WASP-12 b

4.1 Could the ephemeris of WASP-12 b be explained by color-dependent transit times?

Starspots are "blemishes" on the surface of a star characterized by intense magnetic activity. These starspots appear dark because they are relatively cooler than the rest of the photosphere (see Strassmeier 2009 for a review). When an exoplanet transits over a starspot, an anomalous brightening is seen as a positive "bump" in the light-curve. These "bumps" have turned out to be somewhat of a double-edged sword in exoplanetary science. While starspots have helped uncover a host of stellar system properties like stellar rotational velocities (see for e.g. Silva-Valio (2008)), obliquity of the system and consequently the spin-orbit misalignment (see for e.g. Sanchis-Ojeda & Winn 2011), they have also proven a nuisance for measuring precise transit times(see Ioannidis et al. 2017; Tregloan-Reed et al. 2013). A starspot occultation can distort a light-curve, inducing systematic shifts in the best-fit parameters including the mid-transit time.

Ioannidis et al. (2017), argued that starspot occultation by a planet can result in a significant shift in measured mid-transit times of up to 1% of the total transit duration. The transit duration of WASP-12 b is $\sim$ 180 minutes which puts an upper limit on starspots

induced TTVs at $\sim$ 1.8 minutes. In figure 3-3, we see that the orbital decay "amplitude" is of the order of 2 minutes, which means starspots induced TTVs cannot be ruled out just on the basis of observed amplitude of TTVs.

According to its measured spin-orbit misalignment $\lambda(^0) = 59^{+15}_{-20}$ and a relatively low vsin(i) = 2.2 ± 1.5 km/s for a star of temperature 6300 K (Albrecht et al. 2012; Hebb et al. 2009), there's some evidence that we may be observing WASP-12 from nearly above one of its rotation poles. Under this hypothesis, the decadal trend in the apparent period may be the result of a long-term magnetic activity cycle of WASP-12, with a slowly varying spot pattern near the pole of the star. However, the shape and size of a starspot "bump" depends on the wavelength in which the light-curve was obtained. Therefore, a possible way to test the effect of starspots on the transit times of WASP-12 b is to observe several transits in different filters to check whether transit times depend systematically on wavelength in which they were observed.

We collaborated with Norio Narita et al. who have developed a multicolor simultaneous camera called MuSCAT for the 1.88 m telescope at the Okayama Astrophysical Observatory in Japan (see Narita et al. 2015 for more details). MuSCAT can simultaneously observe a single transit in three different filters $g^{'}$ (400-550 nm), $r^{'}$ (550-700 nm) and z_s (820-920 nm). Three transits of WASP-12 b were observed in the above 3 filters on Jan-27-2017, Feb-12-2018 and Feb-13-2018. All 9 light curves were fitted independently with the Mandel and Agol (2009) model following the procedure described in Chapter 2. The quadratic limb-darkening coefficients were tabulated using Claret and Bloemen (2011) and held fixed at $g^{'}$: $u_1 = 0.49$, $u_2 = 0.27$; $r^{'}$: $u_1 = 0.32$, $u_2 = 0.32$; z_s: $u_1 = 0.19$, $u_2 = 0.31$. The light-curves were decorrelated with airmass and measured centroid positions X, Y of the star WASP-12. Figure 4-1 shows the light-curves and the best-fit models. The light-curves obtained on Jan-27-2017 were affected by clouds during egress. The outlying data points were removed from the light-curve before fitting the model. Figure 4-2 shows the positions of those mid-transit times on a plot of timing residuals.

There is no clear evidence for systematic effect of color on transit times, though the data are not good enough yet to rule out this effect at a 1-minute level. Most timing points agree with the orbital decay model. Light-curves in the z_s filter have the highest out-of-transit

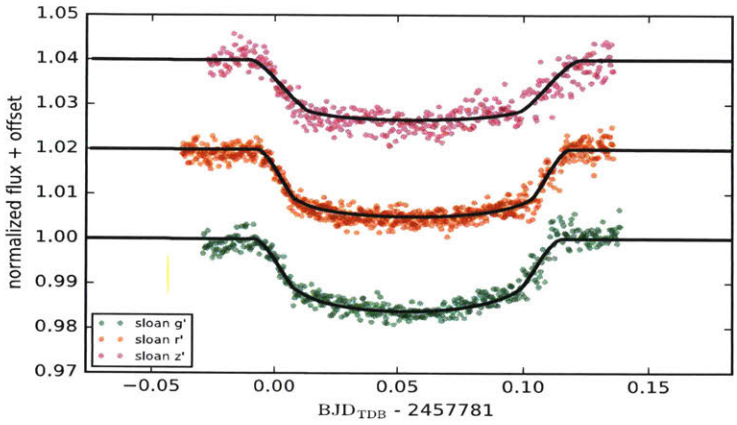

(a) Jan-27-2017

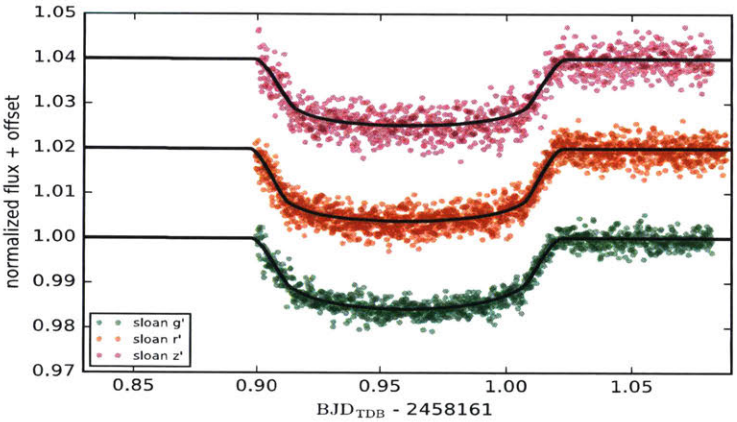

(b) Feb-12-2018

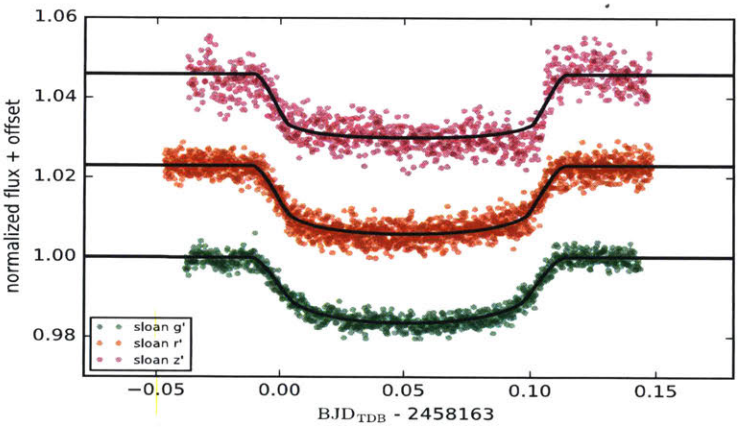

(c) Feb-13-2018

Figure 4-1: WASP-12 b light-curves obtained by MuSCAT and their corresponding best-fit models

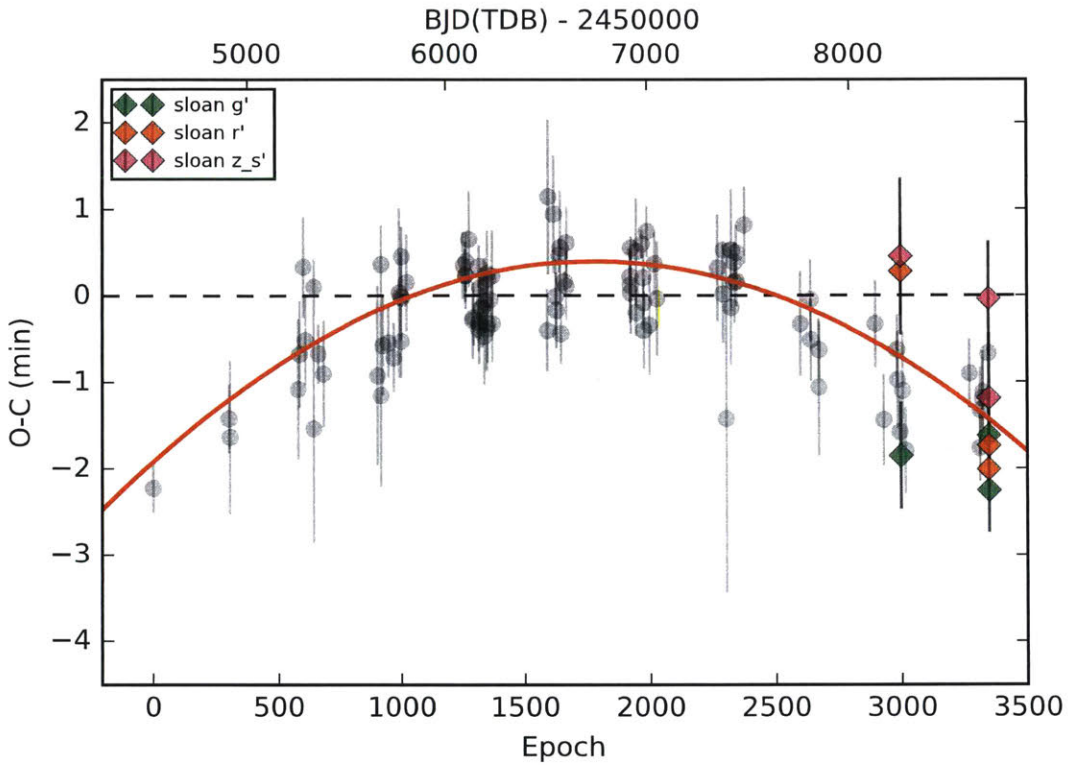

Figure 4-2: Timing residuals for WASP-12 b. The colored points represent the new data points from MuSCAT. The red line is best-fit orbital decay model.

noise among the three filters and therefore are more susceptible to spurious night-to-night timing variations. The transit times on Jan-27-2017 are inconsistent with each other, perhaps because of the clouds interference during egress. To confidently rule out the effect of color on transit times, we need at least 4-5 more such transits.

4.2 Nodal Precession in WASP-12 b

Note: The work presented in this section was made possible with extensive inputs from Nevin Weinberg.

4.2.1 Change in transit period due to nodal precession

Consider a planet whose orbital angular momentum $\boldsymbol{L}_p$ is misaligned with the spin angular momentum $\boldsymbol{L}_s$ of its host star. The total angular momentum $\boldsymbol{L} = \boldsymbol{L}_p + \boldsymbol{L}_s$ is constant and

$L_p \sin i_p = L_s \sin i_s$, where i_p and i_s are the angles between $\boldsymbol{L}$ and the orbital and spin axes. The torque τ due to the stellar quadrupole causes the $L_p \sin i_p$ component of the planet's angular momentum to precess at a rate (Miralda-Escude 2002)

$$\dot{\Omega} \sin i_p = \frac{\tau}{L_p} = \frac{3nJ_2}{4}\left(\frac{R_s}{a}\right)^2 \sin 2i \simeq 8 \times 10^{-8} n \left(\frac{J_2}{10^{-6}}\right)\left(\frac{a/R_s}{3}\right)^{-2} \sin 2i, \tag{4.1}$$

where $i = i_s + i_p$, $n = (GM_s/a^3)^{1/2}$ is the orbital angular frequency, a is the semi-major axis, and R_s, M_s, and J_2 are the radius, mass, and quadrupole moment of the star.

Let $f_m = f_m(\Omega, i_p, ...)$ be the phase in the orbital plane at mid-transit, where Ω is the precessing line of nodes. The next section derives f_m; it's a function of a bunch of sines/cosines and is ~ 1 for a range of viewing geometries. Between two successive mid-transits at times t_1 and t_2, the line of nodes changes by an amount $\Delta\Omega = (\Omega_2 - \Omega_1) = P\dot{\Omega}$, where $P = 2\pi/n$. Assuming the precession per orbit is small,

$$f_m(\Omega_2) = f_m(\Omega_1 + \Delta\Omega) \simeq f_m(\Omega_1) + \frac{df_m}{d\Omega}\Delta\Omega. \tag{4.2}$$

The time between the two consecutive transits (i.e., the transit period) is therefore

$$P_t = t_2 - t_1 = \frac{P}{2\pi}\{1 - [f_m(\Omega_2) - f_m(\Omega_1)]\} = \frac{P}{2\pi}\left[1 - \frac{df_m}{d\Omega}\Delta\Omega\right] \tag{4.3}$$

and the transit period changes at a rate

$$\dot{P}_t = -\frac{P}{2\pi}\frac{d^2 f_m}{d\Omega^2}\frac{d\Omega}{dt}\Delta\Omega = -2\pi\left(\frac{\dot{\Omega}}{n}\right)^2 \frac{d^2 f_m}{d\Omega^2} \simeq 4 \times 10^{-14}\left(\frac{J_2}{10^{-6}}\right)^2\left(\frac{a/R_s}{3}\right)^{-4} \tag{4.4}$$

where I used the scaling from equation (4.1) and took $d^2 f_m/d\Omega^2 \simeq \sin 2i \simeq 1$.

Transit timing measurements of WASP-12 find $|\dot{P}| \simeq 30$ ms yr$^{-1} \simeq 10^{-9}$. Since $a \simeq 3R_s$, attributing $\dot{P}$ to nodal precession requires $J_2 \simeq 2 \times 10^{-4}$. We calculate J_2 in Section 4.2.4, where we show that it scales as $J_2 \propto (\omega_s/\omega_0)^2$, where ω_s is the spin frequency of the star and $\omega_0 = (GM_s/R_s^3)^{1/2}$ is the dynamical frequency. For the sun, $P_s \approx 25$ day and $J_2 \simeq 2 \times 10^{-7}$ (with a factor of a few uncertainty). Scaling to the main sequence models of WASP-12

($R_s = 1.6R_\odot, M = 1.3M_\odot$) then gives

$$J_2 \approx 4 \times 10^{-4} \left(\frac{P_s}{1 \text{ day}}\right)^{-2}. \tag{4.5}$$

This agrees with the more detailed estimate in Section 4.2.4.

For $P_s = 1$ day, have $v_s = 2\pi R_s/P_s = 81$ km s^{-1}. Observations constrain $v_s \sin I_s \lesssim 4$ km s^{-1}, where I_s is relative to the line-of-sight ($I_s \neq i_s$). A $v_s \simeq 80$ km s^{-1} would require $I_s \lesssim 3°$. The probability of seeing the star so close to pole-on is $1 - \cos I_s \simeq 10^{-3}$.

4.2.2 Rotation Periods of stars like WASP-12

McQuillan et al (2014) derive the rotation periods of 34,000 Kepler main sequence stars with $T_{\text{eff}} < 6500$ K. The figures below show the measured rotation periods for stars that match WASP-12 ($T_{\text{eff}} = 6300 \pm 150K, \langle\rho\rangle = 0.475 \pm 0.038$ g cm^{-3}). The different colors are for different ranges in T_{eff} and the second plot zooms in on short periods. Many of the stars have rotation periods $P_s < 2$ days and some even have $P_s < 1$ day.

4.2.3 Variation of orbital phase at mid-transit $f_m(\Omega)$

Let the reference coordinate system be centered on the star (See Murray & Dermott Fig. 2.13), with the z-axis aligned with the total angular momentum $\boldsymbol{L} = \boldsymbol{L}_p + \boldsymbol{L}_s$. Let the planet be at (θ, ϕ, r) and the observer at (θ_0, ϕ_0, d). Then the angle between observer and orbit is

$$\begin{aligned} \cos\gamma &= (\sin\theta\cos\phi\hat{\boldsymbol{x}} + \sin\theta\sin\phi\hat{\boldsymbol{y}} + \cos\theta\hat{\boldsymbol{z}}) \cdot (\sin\theta_0\cos\phi_0\hat{\boldsymbol{x}} + \sin\theta_0\sin\phi_0\hat{\boldsymbol{y}} + \cos\theta_0\hat{\boldsymbol{z}}) \\ &= \sin\theta_0\left(\cos\phi_0\frac{x}{r} + \sin\phi_0\frac{y}{r}\right) + \cos\theta_0\frac{z}{r}, \end{aligned} \tag{4.6}$$

where (x, y, z) are the cartesian coordinates of the planet. From Murray & Dermott 2.122, we can relate the position of the planet in the reference frame to the position in the orbital

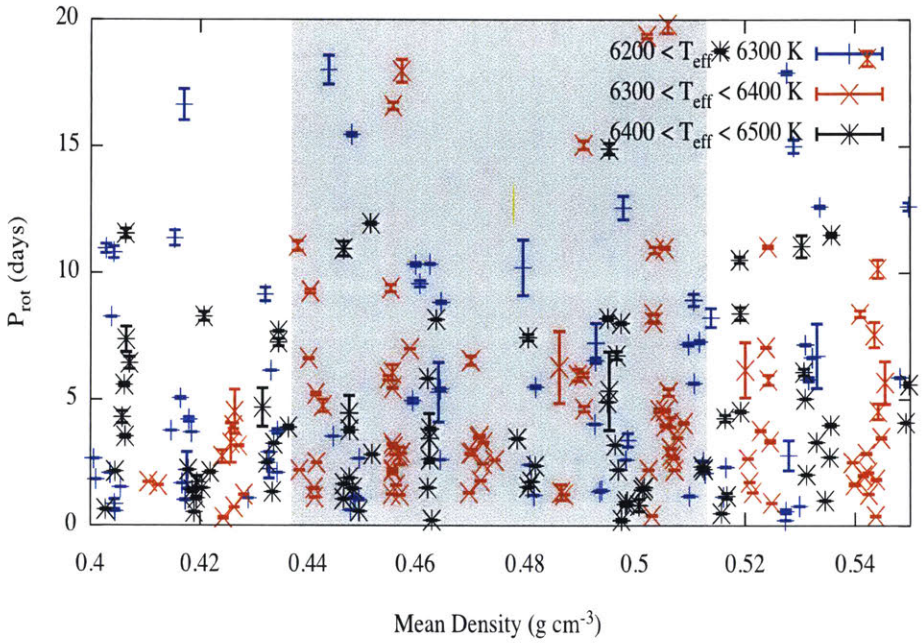

frame through the transformation

$$\begin{pmatrix} x \\ y \\ z \end{pmatrix} = r \begin{pmatrix} \cos\Omega\cos(\omega+f) - \sin\Omega\sin(\omega+f)\cos i_p \\ \sin\Omega\cos(\omega+f) + \cos\Omega\sin(\omega+f)\cos i_p \\ \sin\phi\sin i_p \end{pmatrix}, \tag{4.7}$$

where the various angles are the same as fig. 2.13 of Murmott, shown above (with $I = i_p$; note that the angles are relative to the $\boldsymbol{L}$ reference system, not the observer). Then

$$\cos\gamma = \sin\theta_0\left[\cos(\omega+f)\cos(\phi_0-\Omega) + \sin(\omega+f)\left(\cos i_p \sin(\phi_0-\Omega) + \sin i_p \cot\theta_0\right)\right]. \tag{4.8}$$

Maximize $\cos\gamma$ with respect to f to find the phase at mid-transit $f = f_m$,

$$\begin{aligned} 0 &= \frac{\partial\cos\gamma}{\partial f} \\ &= \sin\theta_0\left[-\sin(\omega+f)\cos(\phi_0-\Omega) + \cos(\omega+f)\left(\cos i_p\sin(\phi_0-\Omega) + \sin i_p\cot\theta_0\right)\right] \end{aligned} \tag{4.9}$$

from McQuillan+14: Rotation Periods of 34,030 Kepler Main-sequence Stars

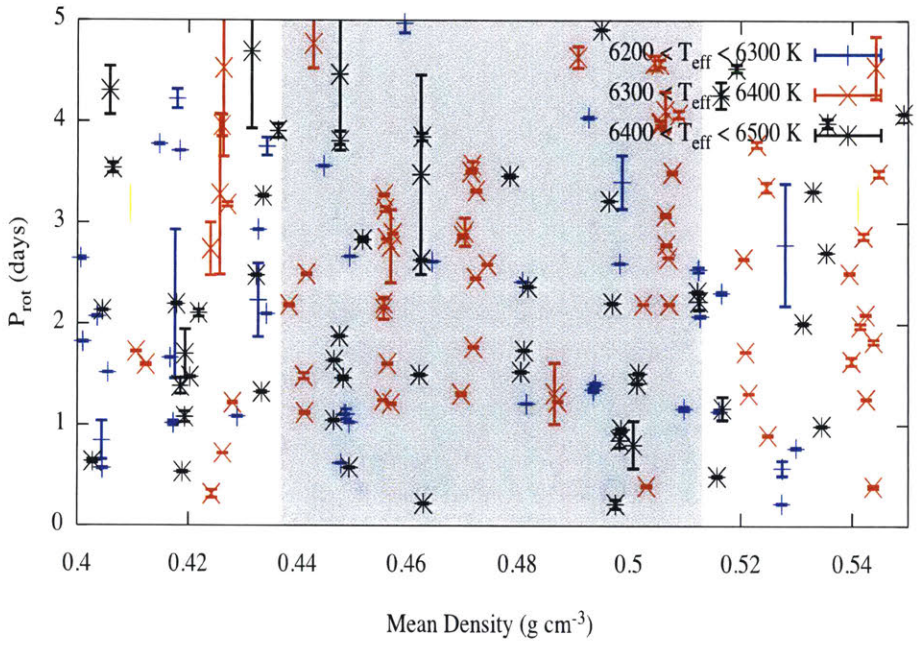

Therefore, the mid-transit occurs at

$$\tan(\omega + f_m) = \cos i_p \tan(\phi_0 - \Omega) + \sin i_p \cot\theta_0 \sec(\phi_0 - \Omega) \tag{4.10}$$

i.e.,

$$f_m(\Omega) = -\omega + \tan^{-1}\left[\cos i_p \tan(\phi_0 - \Omega) + \sin i_p \cot\theta_0 \sec(\phi_0 - \Omega)\right]. \tag{4.11}$$

Plugging back into $\cos\gamma$ to get the value at mid-transit, find

$$\cos\gamma_m = \sin\theta_0 \cos(\phi_0 - \Omega)\sqrt{1 + \left[\cos i_p \tan(\phi_0 - \Omega) + \sin i_p \cot\theta_0 \sec(\phi_0 - \Omega)\right]^2} \tag{4.12}$$

Note that the planet is only observed to transit if the impact parameter

$$b = a\sin\gamma_m < R_s \tag{4.13}$$

or equivalently

$$\cos\gamma_m > \sqrt{1-\left(\frac{R_s}{a}\right)^2}. \tag{4.14}$$

We want $\dot{P}_t \propto d^2 f_m/d\Omega^2$; from mathematica

$$\begin{aligned}\frac{d^2 f_m}{d\Omega^2} &= \frac{\sin(i_p)\sec^2(\Omega-\phi_0)}{8\left(1+[\cos i_p \tan(\phi_0-\Omega)+\sin i_p \cot\theta_0 \sec(\phi_0-\Omega)]^2\right)^2}\times \\ &\times\Big\{\cot\theta_0\sec(\Omega-\phi_0)\Big[2-10\cos 2i_p-2\cos(2[\Omega-\phi_0]) \\ &\qquad +\cos(2[i_p+\Omega-\phi_0])+\cos(2[i_p-\Omega+\phi_0])\Big] \\ &\quad +8\sin^2 i_p\cot^3(\theta_0)\sec(\Omega-\phi_0)-8\sin 2i_p\tan(\Omega-\phi_0)\Big\}\end{aligned} \tag{4.15}$$

Numerical evaluation shows that $d^2 f_m/d\Omega^2 \simeq 0.5$ over a fairly broad range of viewing geometries (its maximum is about 0.65).

4.2.4 Magnitude of J_2

It can be shown that (see Zahn et al. 2010; also, compare Lai, Bildsten, & Kaspi 1995 and Miralda-Escude 2002)

$$\begin{aligned}J_2 &= \frac{2}{3}k_2\left(\frac{\omega_s}{\omega_0}\right)^2 \\ &\simeq 3\times10^{-4}\left(\frac{k_2}{0.01}\right)\left(\frac{P_s}{1\text{ day}}\right)^{-2}\left(\frac{M_s}{1.3M_\odot}\right)^{-1}\left(\frac{R_s}{1.6R_\odot}\right)^3.\end{aligned} \tag{4.16}$$

where k_2 is the apsidal motion constant and in the second line we plugged in a value of $k_2 \simeq 0.01$ for WASP-12 based on the tables of stellar models in Claret & Gimenez (1998).

4.2.5 Results

We loop over all values of θ_0, i_p, Ω, and ϕ_s, where the first three are defined above and ϕ_s is the longitude of the stellar spin axis relative to the z-axis (i.e., relative to $\hat{\boldsymbol{L}}$). We chose the orientation of the x-y axes such that the observer is located at $\phi_0 = \pi/2$ (i.e., the x-axis is perpendicular to the line-of-sight; like in fig. 1 of Lai, Bildsten, & Kaspi 1995). For given

values of P_s, M_s, R_s, M_p, and a, we first calculate i_s using the relation

$$L_s \sin i_s = L_p \sin i_p, \tag{4.17}$$

where $L_s = k^2 M_s R_s^3 \omega_s$, $k^2 = 0.1$ (Miralda-Escude 2002), and $L_p = M_p n a^2$. This then gives $i = i_p + i_s$ and

$$\dot{\Omega} = \frac{3nJ_2}{4}\left(\frac{R_s}{a}\right)^2 \frac{\sin 2i}{\sin i_p}. \tag{4.18}$$

We calculate $\cos\gamma_m$ using eq. (4.12), and only consider the transiting cases, i.e., those that satisfy $\cos\gamma_m > [1-(R_s/a)^2]^{1/2}$. We then evaluate $d^2 f_m/d\Omega^2$ (eq. 4.15) and

$$\dot{P}_t = -2\pi\left(\frac{\dot{\Omega}}{n}\right)^2 \frac{d^2 f_m}{d\Omega^2}, \tag{4.19}$$

which we can compare to the measured value for WASP-12 of

$$\dot{P} = -29 \pm 3 \text{ ms yr}^{-1} = -(9.2 \pm 1.0) \times 10^{-10}. \tag{4.20}$$

We can also restrict consideration to those angles that agree with the constraints on the orbital and spin inclination, I_p and I_s, relative to the line-of-sight. The inclination of the star's spin-axis $\hat{\boldsymbol{L}}_s$ relative to the line-of-sight $\hat{\boldsymbol{n}}$ is given by

$$\begin{aligned}
\cos I_s &= \hat{\boldsymbol{L}}_s \cdot \hat{\boldsymbol{n}} \\
&= (\sin i_s \cos\phi_s \hat{\boldsymbol{x}} + \sin i_s \sin\phi_s \hat{\boldsymbol{y}} + \cos i_s \hat{\boldsymbol{z}}) \cdot (\sin\theta_0 \cos\phi_0 \hat{\boldsymbol{x}} + \sin\theta_0 \sin\phi_0 \hat{\boldsymbol{y}} + \cos\theta_0 \hat{\boldsymbol{z}}) \\
&= \sin i_s \sin\theta_0 \cos(\phi_s - \phi_0) + \cos i_s \cos\theta_0.
\end{aligned} \tag{4.21}$$

From this we calculate $v_s \sin I_s$, where $v_s = 2\pi R_s/P_s$, and compare to the measured value for WASP-12 of $v_s \sin I_s < 2.2 \pm 1.5$ km s^{-1}. In practice, to get a large enough $\dot{P}_t$ we need $P_s \lesssim 1$ day, which implies $I_s \simeq 0$ (i.e., we're seeing the star nearly pole on). The probability of such an orientation is then $1 - \cos I_s \simeq I_s^2/2 \ll 1$.

Similarly, we compute the inclination of the orbit relative to the line-of-sight

$$\begin{aligned}
\cos I_p &= \hat{\boldsymbol{L}}_p \cdot \hat{\boldsymbol{n}} \\
&= (\sin i_p \cos\phi_p \hat{\boldsymbol{x}} + \sin i_p \sin\phi_p \hat{\boldsymbol{y}} + \cos i_s \hat{\boldsymbol{z}}) \cdot (\sin\theta_0 \cos\phi_0 \hat{\boldsymbol{x}} + \sin\theta_0 \sin\phi_0 \hat{\boldsymbol{y}} + \cos\theta_0 \hat{\boldsymbol{z}}) \\
&= \sin i_p \sin\theta_0 \cos(\phi_p - \phi_0) + \cos i_p \cos\theta_0 \\
&= -\sin i_p \sin\theta_0 \cos\Omega + \cos i_p \cos\theta_0, \qquad (4.22)
\end{aligned}$$

where in the last line we used the fact that $\phi_0 = \pi/2$ and $\phi_p = -\pi/2 + \Omega$ (again see fig. 1 in Lai, Bildsten, & Kaspi 1995 and their eq. 6). We can compare this with the measured value $I_p = 86.2 \pm 3.0$ deg.

The figures below show I_p vs. $1 - \cos I_s$ for different values of P_s and k_2 for cases with large enough $\dot{P}$ and small enough $v_s \sin I_s$. We need small P_s to get large enough $\dot{P}$ and I_p. However, the smaller P_s, the smaller I_s needs to be to get $v_s \sin I_s \lesssim 4$ km s^{-1}. If $k_2 \approx 0.01$, need $P_s \lesssim 0.5$ day, in which case $1 - \cos I_s \lesssim 10^{-4}$. Only if $k_2 \approx 0.1$, about 10 times the expected value, is the probability $1 - \cos I_s > 10^{-3}$ and $I_p \simeq 85°$.

4.2.6 Impact parameter to differentiate between nodal precession and orbital decay

The impact parameter b, is the shortest distance (in units of stellar radii) from the center of a stellar disk and te chord that defines the path of a transiting planet and is defined as $b \equiv \frac{a\ cos(i)}{R_*}$. Given the observed $\dot{P} = -29 \pm 3$ ms yr^{-1} in WASP-12 b, we find that if the orbit is undergoing nodal precession, then we expect a change in impact parameter $\Delta b \sim 0.1$ over 10 years of observation baseline. However, for the orbital decay model the expected $\Delta b \sim 0.01$. The difference lies in the contribution to Δb in the two scenarios. In orbital decay we expect impact parameter to change because the orbit is shrinking, and therefore the semi-major axis a decreases. In nodal precession, however, impact parameter changes because of changing orbital inclination, i. Therefore, precise measurements of b over time may be the easiest way to differentiate between these two models.

Impact parameter is a free parameter during the fitting of model to a light curve. Fig.

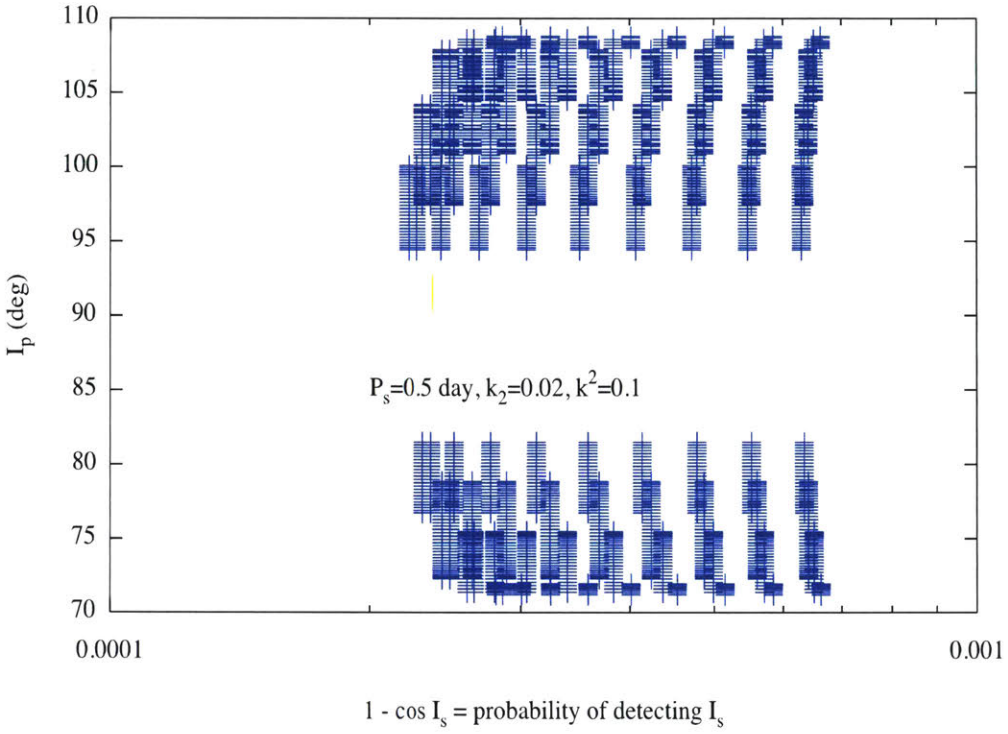

4-3 shows the best-fit b over several epochs. We see that the observed b have too large uncertainties to judge by eye if there is a trend over time. For a more quantitative analysis, we grouped together five good quality light curves between epochs 500-800 and five light curves from the latest season. The mean of impact parameters in each group was calculated and compared. For the first group we found $b_i = 0.29 \pm 0.09$ whereas for the second group we found $b_f = 0.33 \pm 0.06$. The difference in impact parameter is not statistically significant at the current precision on b. Therefore, we cannot definitively rule out nodal precession based on impact parameter measurements alone. One of the possible reasons for such poor precision on b is the fact that there exists a degeneracy between b and R_*/a because both are free parameters during light curve fitting. Fig. 4-4 shows a typical correlation plot between different parameters during a MCMC run. The $b-R_*/a$ box shows strong correlation between them. To better constrain b, highly precise light curves are required, that TESS promises to deliver in the near future. See Chapter 5 for a brief discussion on TESS.

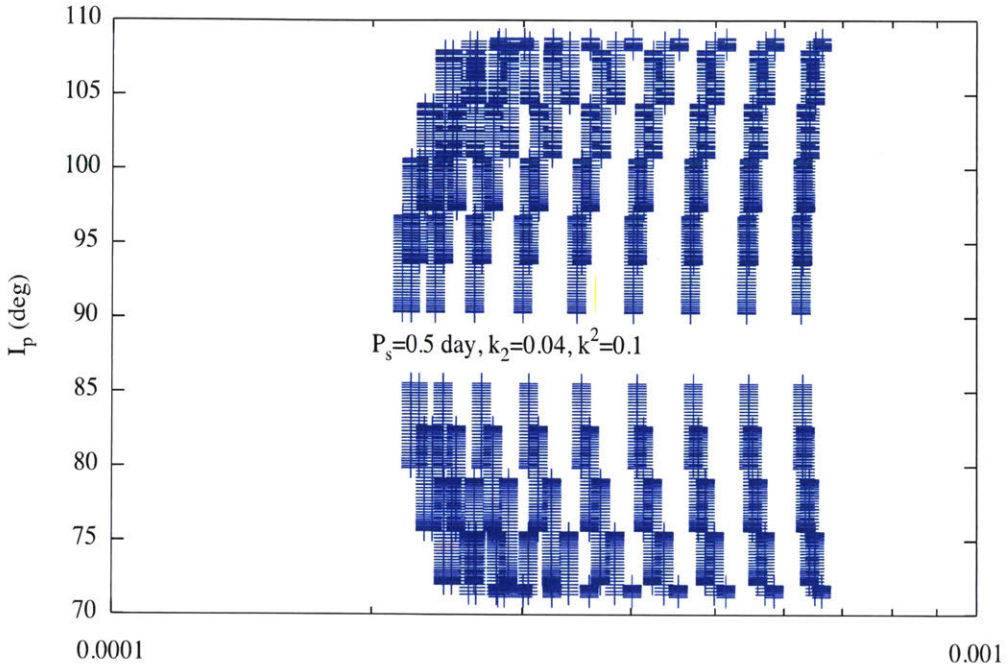
110
105
100
95
90
85
80
75
70
I_p (deg)
P_s=0.5 day, k_2=0.04, k^2=0.1
0.0001
0.001
1 - cos I_s = probability of detecting I_s

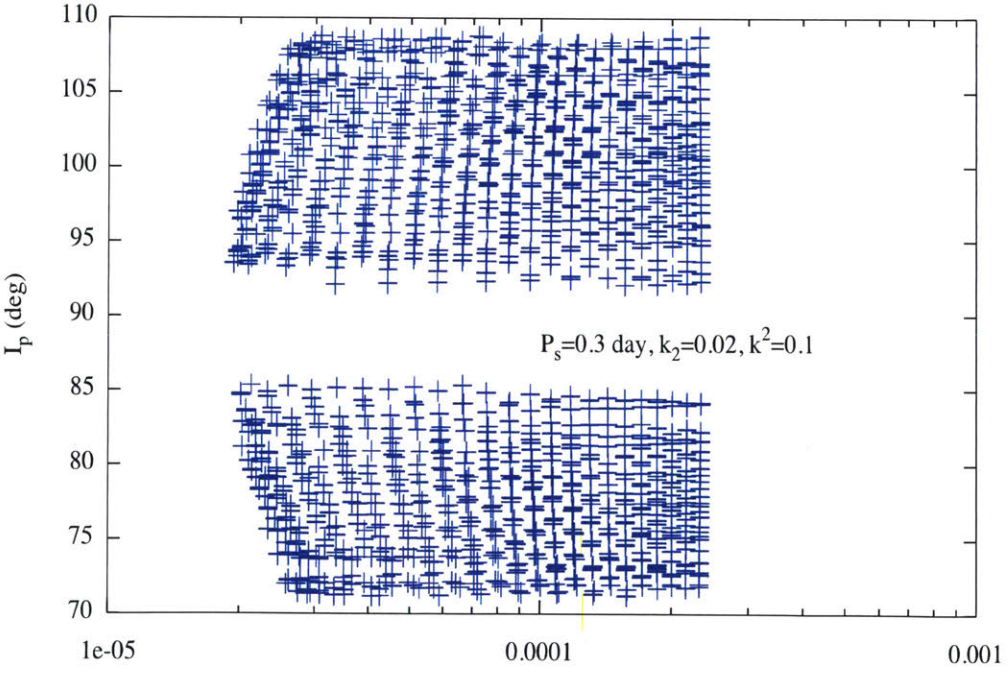
110
105
100
95
90
85
80
75
70
I_p (deg)
P_s=0.3 day, k_2=0.02, k^2=0.1
1e-05
0.0001
0.001
1 - cos I_s = probability of detecting I_s

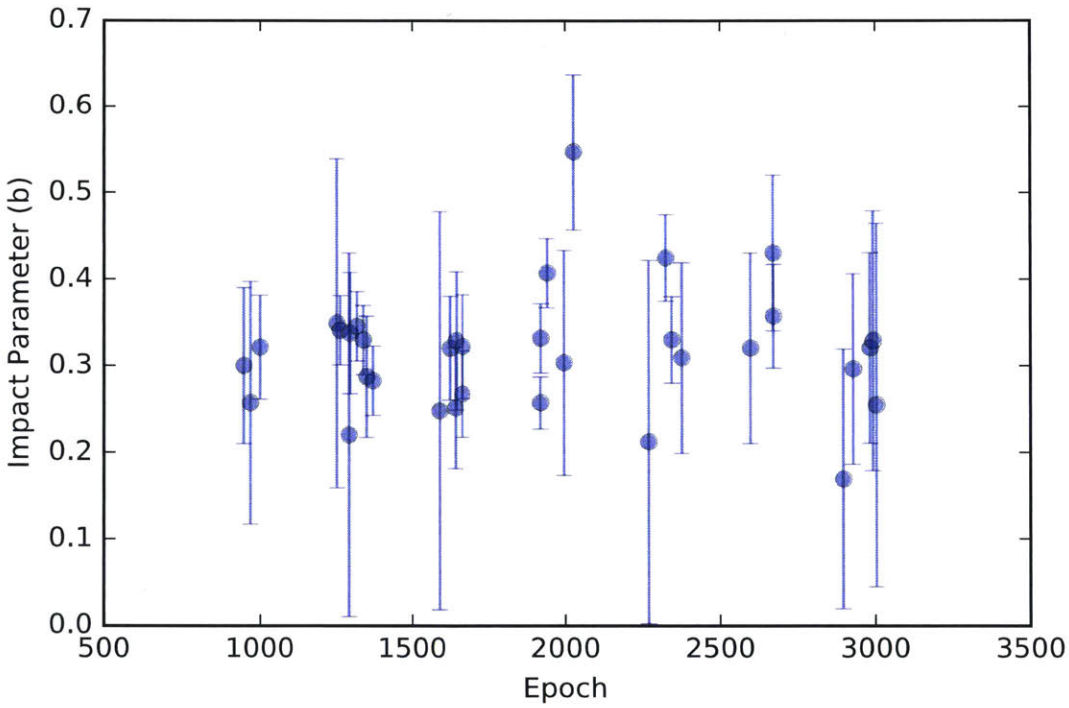

Figure 4-3: Observed impact parameters for WASP-12 b.

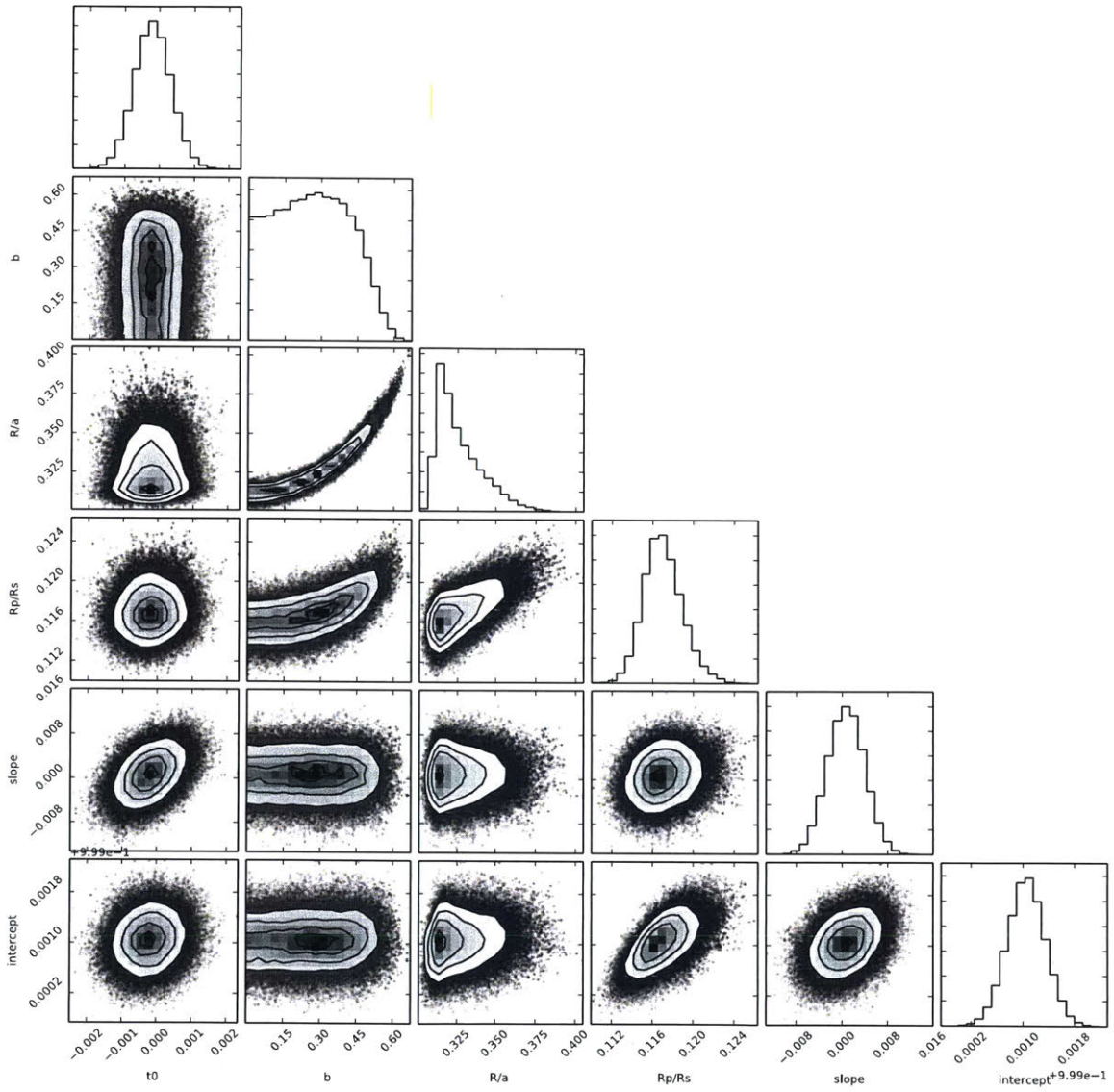

Figure 4-4: A typical correlation plot between the fitting parameters that describe the Mandel & Agol 2002 transit model.

Chapter 5

Summary And Future Work

5.1 Progress so far on orbital decay

This project's goal is to systematically search for orbital decay in exoplanets. We have narrowed down our search to 12 best targets that we have collected transit times on and intend to continue monitoring in the future. Among the targets, we find that the best candidate currently for orbital decay is WASP-12 b because it has been consistently been monitored for over a decade. As seen in Chapter 3, WASP-12 b deviates from a linear ephemeris and this phenomenon can be interpreted as either orbital decay or apsidal precession of the orbit, with orbital decay being the more statistically favored model. In the following chapter 4, we saw that we also cannot completely rule out nodal precession and color-dependent transit times as an explanation for the observed deviation from linear ephemeris. More continued observations of WASP-12 b are necessary for us to confidently confirm orbital decay. Exciting results lie ahead with many more Hot Jupiters approaching the ripe time for the detection of orbital decay.

The search for orbital decay in other targets is still in its infancy, though a few targets are approaching a decade since its discovery. The goals for these targets is to provide an "anchor" point in transit times for future observations. Being observable only in the southern hemisphere puts some of our best targets including the likes of WASP-19 and WASP-18 at a disadvantage. We plan to remedy this with our collaboration with the LCO Global Telescope Network Key Project. Under this collaboration, we plan on regularly observing the southern

targets in future.

Currently, with the data at hand, the most tight constraint we can put on tidal quality parameter is $Q_* > 2 \times 10^5$, in case of WASP-19 b. If WASP-19 continues to have the same timing dispersion till epoch 5000 (early 2019 in calendar), we may begin to probe limits $Q_* > 2 \times 10^6$, which will be a lot more useful constraint.

Another exciting opportunity for orbital decay is the upcoming space missions like TESS and JWST. The Transiting Exoplanet Survey Satellite (TESS) was launched on April 18, 2018 with the goal of detecting new exoplanets. Unlike the Kepler, TESS is an all-sky survey satellite with the principal goal "to detect small planets with bright host stars in the solar neighborhood, so that detailed characterizations of the planets and their atmospheres can be performed" (Ricker et al. 2014). Over its two-year mission, TESS will monitor over 200,000 stars searching for planetary transits. TESS is expected to catalog more than 1500 new transiting exoplanets. Over its mission course, TESS will also observe most of our targets for orbital decay, providing high quality light-curves and therefore, high-precision transit times. The TESS light curves will be free of the confounding effects of earth's atmosphere which means the night-to-night random spurious deviations in transit times will be minimized. These highly reliable and precise transit times will be of great help in the future for the detection of orbital decay. In light of nodal precession model, TESS light curves can also help us better constrain the impact parameter of WASP-12 b. Having both an accurate and precise impact parameter will help in differentiating between the nodal precession and orbital decay model.

5.2 Upper limit on eccentricity of Hot Jupiters from transit times

This section explores a by-product of the apsidal precession model in WASP-12 b - constraining eccentricity of Hot Jupiters using transit times. Eccentricity of an exoplanetary orbit can be determined from the star's radial velocity (RV) measurements over time (See Husnoo et al. 2012 for e.g.). The shape of RV versus time for an exoplanet in an eccentric

orbit will significantly deviate from a sinusoid for a planet in a circular orbit, thus enabling putting a limit on eccentricity of the planet's orbit. For example, Husnoo et al. (2012) found for WASP-12 b an eccentricity of $e = 0.049 \pm 0.015$ and Bakos et al. (2011) estimated $e = 0.106 \pm 0.044$ for HAT-P-23 b. Similarly, for a lot of Hot Jupiters the upper limits range from 0.01 - 0.1. Knowing the eccentricity of an exoplanet is crucial in understanding many star-planet interactions, including the likes of apsidal precession and tidal circularization.

We saw in Chapter 3 that Eqn. 7 describes the transit ephemeris of a planet in slightly eccentric orbit and undergoing apsidal precession:

$$t_{\rm tra}(E) = t_0 + P_{\rm s}E - \frac{eP_{\rm a}}{\pi}\cos\omega \tag{5.1}$$

where ω is a function of epoch E and the rate of precession $\frac{d\omega}{dE}$

$$\omega(E) = \omega_0 + \frac{d\omega}{dE}E, \tag{5.2}$$

Rearranging the same equation we see that:

$$t_{\rm tra}(E) - (t_0 + P_{\rm s}E) = -\frac{eP_{\rm a}}{\pi}\cos\omega \tag{5.3}$$

The left-hand side is the definition of timing residuals from a linear ephemeris, i.e. the observed transit time minus the calculated transit time. The right hand side is basically a sinusoidal function where e determines only the amplitude. Therefore, fitting sinusoidal functions to the O-C might provide upper limits on the eccentricity. Note that this method requires an apsidally precessing orbit but does not require the knowledge of the cause of such precession. Another important observation is that since the anomalistic period P_a, is a function of the precession rate $\frac{d\omega}{dE}$ (see Eqn. 3.10), there exists a degeneracy between e and $\frac{d\omega}{dE}$ in determining the amplitude of the fitted sinusoid, which could potentially contaminate the limit on eccentricity. Therefore, to break this degeneracy, it is necessary to have at least some periodic variation in the timing residuals such that $\frac{d\omega}{dE}$ can be fixed by the periodicity of timing residuals.

In Chapter 2, we saw that only WASP-12 and HAT-P-23 currently show hints of pe-

riodic variation in its O-C. We fitted a sine function to those two O-C plots using the MCMC algorithm. The model had 3 free parameters: eccentricity e, precession rate $\frac{d\omega}{dE}$ and argument of pericenter ω_0. Then we increased the eccentricity in small steps until the χ^2 of the fit became no longer tenable. We defined the boundary for "no tenability" as when $\chi^2 > aN_{dof} + 3\sqrt{2aN_{dof}}$, where N_{dof} is the number of degrees of freedom. The best-fit will generally not result in $\chi^2 = N_{dof}$ because of either underestimation or overestimation of errors in the data. The constant a,thus helps in scaling the best-fit χ^2 to N_{dof}. The quantity $2N_{dof}$ is the variance and N_{dof} is the mean of a χ^2 distribution. It is worthy to note that the "best-fit" eccentricity alone may not be reliable if the data are not sufficient in quantity or if there are better competing models than apsidal precession. Therefore, the next best option is to, using the above threshold, put approximately a 3σ upper limit on the eccentricity of the planet's orbit. Fig. 5-1 and Fig. 5-2 show the sinusoidal fit to timing residuals. By following the above threshold, we found the following 3σ upper limits on the eccentricities of WASP-12 and HAT-P-23,

1) WASP-12: $e < 0.003$

2) HAT-P-23: $e < 0.010$

Note that the above upper limits are more constraining than limits from the radial velocity method by an order of magnitude or better. While potentially better constraints on eccentricity might be achieved, the major shortcoming of using transit times is that this method is only valid for targets that have been consistently observed over more than a decade and also show possible signs of periodicity in the transit times to constrain precession rate. Thus, this method may prove effective in future when many Hot Jupiters would have accumulated enough transit times over a longer time baseline. Furthermore, in case of HAT-P-23, the one season with deviant transit times may just be caused by starspots, resulting in false constraint on eccentricity. Therefore, consistent monitoring of these targets is necessary in the future.

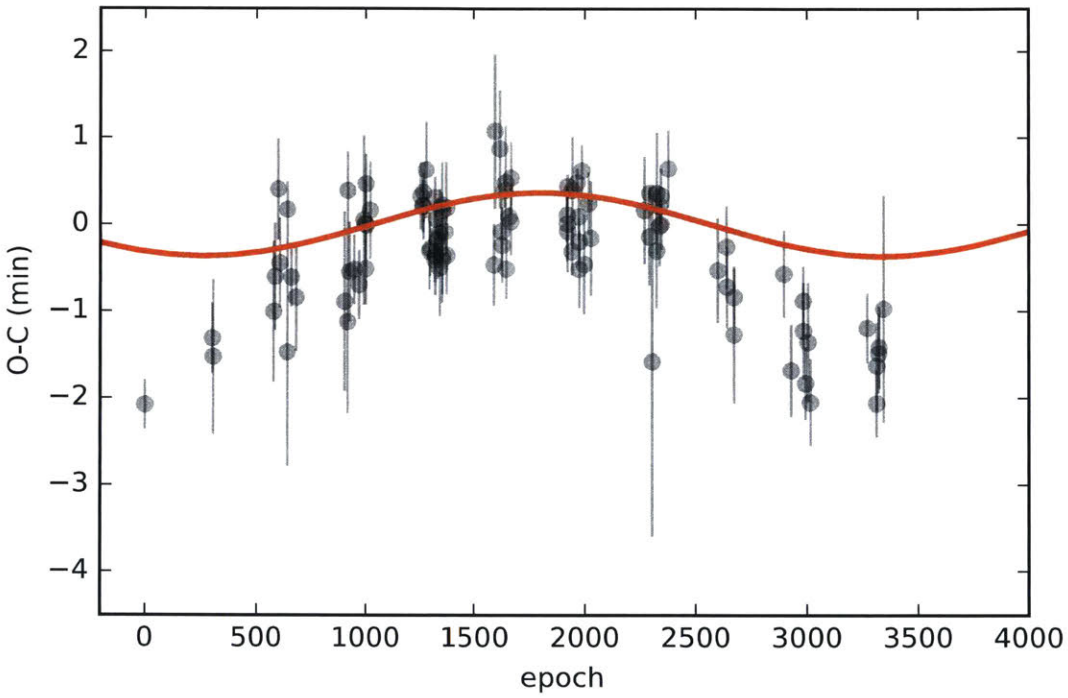

Figure 5-1: A sinusoid fit to WASP-12 b timing residuals

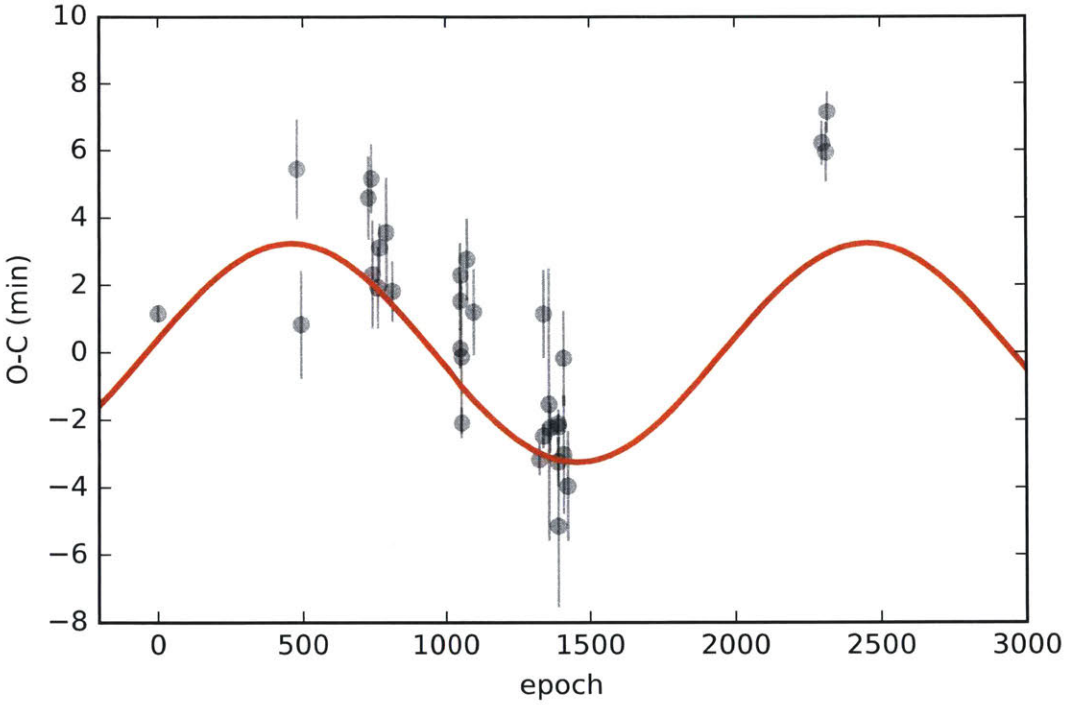

Figure 5-2: A sinusoid fit to HAT-P-23 b timing residuals

Bibliography

S. Albrecht, J. N. Winn, J. A. Johnson, A. W. Howard, G. W. Marcy, R. P. Butler, P. Arriagada, J. D. Crane, S. A. Shectman, I. B. Thompson, T. Hirano, G. Bakos, and J. D. Hartman. Obliquities of Hot Jupiter Host Stars: Evidence for Tidal Interactions and Primordial Misalignments. , 757:18, September 2012. doi: 10.1088/0004-637X/757/1/18.

D. W. Allan. Statistics of atomic frequency standards. *IEEE Proceedings*, 54, February 1966. doi: 10.1109/PROC.1966.4634.

J. H. Applegate. A mechanism for orbital period modulation in close binaries. , 385:621–629, February 1992. doi: 10.1086/170967.

A. J. Barker and G. I. Ogilvie. On internal wave breaking and tidal dissipation near the centre of a solar-type star. , 404:1849–1868, June 2010. doi: 10.1111/j.1365-2966.2010.16400.x.

E. B. Bechter, J. R. Crepp, H. Ngo, H. A. Knutson, K. Batygin, S. Hinkley, P. S. Muirhead, J. A. Johnson, A. W. Howard, B. T. Montet, C. T. Matthews, and T. D. Morton. WASP-12b and HAT-P-8b are Members of Triple Star Systems. , 788:2, June 2014. doi: 10.1088/0004-637X/788/1/2.

D. Bisikalo, P. Kaygorodov, D. Ionov, V. Shematovich, H. Lammer, and L. Fossati. Three-dimensional Gas Dynamic Simulation of the Interaction between the Exoplanet WASP-12b and its Host Star. , 764:19, February 2013. doi: 10.1088/0004-637X/764/1/19.

C. J. Campo, J. Harrington, R. A. Hardy, K. B. Stevenson, S. Nymeyer, D. Ragozzine, N. B. Lust, D. R. Anderson, A. Collier-Cameron, J. Blecic, C. B. T. Britt, W. C. Bowman, P. J. Wheatley, T. J. Loredo, D. Deming, L. Hebb, C. Hellier, P. F. L. Maxted, D. Pollaco, and R. G. West. On the Orbit of Exoplanet WASP-12b. , 727:125, February 2011. doi: 10.1088/0004-637X/727/2/125.

T. Chan, M. Ingemyr, J. N. Winn, M. J. Holman, R. Sanchis-Ojeda, G. Esquerdo, and M. Everett. The Transit Light-curve Project. XIV. Confirmation of Anomalous Radii for the Exoplanets TrES-4b, HAT-P-3b, and WASP-12b. , 141:179, June 2011. doi: 10.1088/0004-6256/141/6/179.

A. Claret and S. Bloemen. Gravity and limb-darkening coefficients for the Kepler, CoRoT, Spitzer, uvby, UBVRIJHK, and Sloan photometric systems. , 529:A75, May 2011. doi: 10.1051/0004-6361/201116451.

K. A. Collins, J. F. Kielkopf, and K. G. Stassun. Transit Timing Variation Measurements of WASP-12b and Qatar-1b: No Evidence Of Additional Planets. , 153:78, February 2017. doi: 10.3847/1538-3881/153/2/78.

C. M. Copperwheat, P. J. Wheatley, J. Southworth, J. Bento, T. R. Marsh, V. S. Dhillon, J. J. Fortney, S. P. Littlefair, and R. Hickman. Transmission photometry of WASP-12b: simultaneous measurement of the planetary radius in three bands. , 434:661–670, September 2013. doi: 10.1093/mnras/stt1056.

N. B. Cowan, P. Machalek, B. Croll, L. M. Shekhtman, A. Burrows, D. Deming, T. Greene, and J. L. Hora. Thermal Phase Variations of WASP-12b: Defying Predictions. , 747:82, March 2012. doi: 10.1088/0004-637X/747/1/82.

B. Croll, L. Albert, R. Jayawardhana, M. Cushing, C. Moutou, D. Lafreniere, J. A. Johnson, A. S. Bonomo, M. Deleuil, and J. Fortney. Near-infrared Thermal Emission Detections of a Number of Hot Jupiters and the Systematics of Ground-based Near-infrared Photometry. , 802:28, March 2015. doi: 10.1088/0004-637X/802/1/28.

I. J. M. Crossfield, T. Barman, B. M. S. Hansen, I. Tanaka, and T. Kodama. Re-evaluating WASP-12b: Strong Emission at 2.315 μm, Deeper Occultations, and an Isothermal Atmosphere. , 760:140, December 2012. doi: 10.1088/0004-637X/760/2/140.

D. Deming, H. Knutson, J. Kammer, B. J. Fulton, J. Ingalls, S. Carey, A. Burrows, J. J. Fortney, K. Todorov, E. Agol, N. Cowan, J.-M. Desert, J. Fraine, J. Langton, C. Morley, and A. P. Showman. Spitzer Secondary Eclipses of the Dense, Modestly-irradiated, Giant Exoplanet HAT-P-20b Using Pixel-level Decorrelation. , 805:132, June 2015. doi: 10.1088/0004-637X/805/2/132.

J. Eastman, R. Siverd, and B. S. Gaudi. Achieving Better Than 1Minute Accuracy in the Heliocentric and Barycentric Julian Dates. , 122:935, August 2010. doi: 10.1086/655938.

J. Eastman, B. S. Gaudi, and E. Agol. EXOFAST: A Fast Exoplanetary Fitting Suite in IDL. , 125:83, January 2013. doi: 10.1086/669497.

R. Essick and N. Weinberg. Orbital decay of hot Jupiters due to nonlinear tidal dissipation within solar-type hosts. In *APS April Meeting Abstracts*, March 2016.

D. Föhring, V. S. Dhillon, N. Madhusudhan, T. R. Marsh, C. M. Copperwheat, S. P. Littlefair, and R. W. Wilson. ULTRACAM z′-band detection of the secondary eclipse of WASP-12b. , 435:2268–2273, November 2013. doi: 10.1093/mnras/stt1443.

D. Foreman-Mackey, D. W. Hogg, D. Lang, and J. Goodman. emcee: The MCMC Hammer. , 125:306, March 2013. doi: 10.1086/670067.

L. Fossati, S. Bagnulo, A. Elmasli, C. A. Haswell, S. Holmes, O. Kochukhov, E. L. Shkolnik, D. V. Shulyak, D. Bohlender, B. Albayrak, C. Froning, and L. Hebb. A Detailed Spectropolarimetric Analysis of the Planet-hosting Star WASP-12. , 720:872–886, September 2010. doi: 10.1088/0004-637X/720/1/872.

A. Giménez and M. Bastero. A Revision of the Ephemeris-Curve Equations for Eclipsing Binaries with Apsidal Motion. , 226:99–107, April 1995. doi: 10.1007/BF00626903.

P. Goldreich and S. Soter. Q in the Solar System. , 5:375–389, 1966. doi: 10.1016/0019-1035(66)90051-0.

J. R. Gott, III. Implications of the Copernican principle for our future prospects. , 363: 315–319, May 1993. doi: 10.1038/363315a0.

B. M. S. Hansen. Calibration of Equilibrium Tide Theory for Extrasolar Planet Systems. , 723:285–299, November 2010. doi: 10.1088/0004-637X/723/1/285.

C. A. Haswell, L. Fossati, T. Ayres, K. France, C. S. Froning, S. Holmes, U. C. Kolb, R. Busuttil, R. A. Street, L. Hebb, A. Collier Cameron, B. Enoch, V. Burwitz, J. Rodriguez, R. G. West, D. Pollacco, P. J. Wheatley, and A. Carter. Near-ultraviolet Absorption, Chromospheric Activity, and Star-Planet Interactions in the WASP-12 system. , 760:79, November 2012. doi: 10.1088/0004-637X/760/1/79.

L. Hebb, A. Collier-Cameron, B. Loeillet, D. Pollacco, G. Hébrard, R. A. Street, F. Bouchy, H. C. Stempels, C. Moutou, E. Simpson, S. Udry, Y. C. Joshi, R. G. West, I. Skillen, D. M. Wilson, I. McDonald, N. P. Gibson, S. Aigrain, D. R. Anderson, C. R. Benn, D. J. Christian, B. Enoch, C. A. Haswell, C. Hellier, K. Horne, J. Irwin, T. A. Lister, P. Maxted, M. Mayor, A. J. Norton, N. Parley, F. Pont, D. Queloz, B. Smalley, and P. J. Wheatley. WASP-12b: The Hottest Transiting Extrasolar Planet Yet Discovered. , 693:1920–1928, March 2009. doi: 10.1088/0004-637X/693/2/1920.

J. S. Heyl and B. J. Gladman. Using long-term transit timing to detect terrestrial planets. , 377:1511–1519, June 2007. doi: 10.1111/j.1365-2966.2007.11697.x.

S. Hoyer, E. Pallé, D. Dragomir, and F. Murgas. Ruling out the Orbital Decay of the WASP-43b Exoplanet. , 151:137, June 2016. doi: 10.3847/0004-6256/151/6/137.

N. Husnoo, F. Pont, T. Mazeh, D. Fabrycky, G. Hébrard, F. Bouchy, and A. Shporer. Observational constraints on tidal effects using orbital eccentricities. , 422:3151–3177, June 2012. doi: 10.1111/j.1365-2966.2012.20839.x.

P. Hut. Stability of tidal equilibrium. , 92:167–170, December 1980.

B. Jackson, R. Greenberg, and R. Barnes. Tidal Evolution of Close-in Extrasolar Planets. , 678:1396-1406, May 2008. doi: 10.1086/529187.

B. Jackson, P. Arras, K. Penev, S. Peacock, and P. Marchant. A New Model of Roche Lobe Overflow for Short-period Gaseous Planets and Binary Stars. , 835:145, February 2017. doi: 10.3847/1538-4357/835/2/145.

A. Jordán and G. Á. Bakos. Observability of the General Relativistic Precession of Periastra in Exoplanets. , 685:543-552, September 2008. doi: 10.1086/590549.

H. A. Knutson, B. J. Fulton, B. T. Montet, M. Kao, H. Ngo, A. W. Howard, J. R. Crepp, S. Hinkley, G. Á. Bakos, K. Batygin, J. A. Johnson, T. D. Morton, and P. S. Muirhead. Friends of Hot Jupiters. I. A Radial Velocity Search for Massive, Long-period Companions to Close-in Gas Giant Planets. , 785:126, April 2014. doi: 10.1088/0004-637X/785/2/126.

L. Kreidberg, M. R. Line, J. L. Bean, K. B. Stevenson, J.-M. Désert, N. Madhusudhan, J. J. Fortney, J. K. Barstow, G. W. Henry, M. H. Williamson, and A. P. Showman. A Detection of Water in the Transmission Spectrum of the Hot Jupiter WASP-12b and Implications for Its Atmospheric Composition. , 814:66, November 2015. doi: 10.1088/0004-637X/814/1/66.

D. Lai, C. Helling, and E. P. J. van den Heuvel. Mass Transfer, Transiting Stream, and Magnetopause in Close-in Exoplanetary Systems with Applications to WASP-12. , 721: 923–928, October 2010. doi: 10.1088/0004-637X/721/2/923.

B. Levrard, C. Winisdoerffer, and G. Chabrier. Falling Transiting Extrasolar Giant Planets. , 692:L9–L13, February 2009. doi: 10.1088/0004-637X/692/1/L9.

N. K. Lewis, H. A. Knutson, A. P. Showman, N. B. Cowan, G. Laughlin, A. Burrows, D. Deming, J. R. Crepp, K. J. Mighell, E. Agol, G. Á. Bakos, D. Charbonneau, J.-M. Désert, D. A. Fischer, J. J. Fortney, J. D. Hartman, S. Hinkley, A. W. Howard, J. A. Johnson, M. Kao, J. Langton, and G. W. Marcy. Orbital Phase Variations of the Eccentric Giant Planet HAT-P-2b. , 766:95, April 2013. doi: 10.1088/0004-637X/766/2/95.

S.-L. Li, N. Miller, D. N. C. Lin, and J. J. Fortney. WASP-12b as a prolate, inflated and disrupting planet from tidal dissipation. , 463:1054–1056, February 2010. doi: 10.1038/nature08715.

M. López-Morales, J. L. Coughlin, D. K. Sing, A. Burrows, D. Apai, J. C. Rogers, D. S. Spiegel, and E. R. Adams. Day-side z'-band Emission and Eccentricity of WASP-12b. , 716:L36–L40, June 2010. doi: 10.1088/2041-8205/716/1/L36.

R. Luger, E. Agol, E. Kruse, R. Barnes, A. Becker, D. Foreman-Mackey, and D. Deming. EVEREST: Pixel Level Decorrelation of K2 Light Curves. , 152:100, October 2016. doi: 10.3847/0004-6256/152/4/100.

G. Maciejewski, R. Errmann, S. Raetz, M. Seeliger, I. Spaleniak, and R. Neuhäuser. High-precision photometry of WASP-12 b transits. , 528:A65, April 2011. doi: 10.1051/0004-6361/201016268.

G. Maciejewski, D. Dimitrov, M. Seeliger, S. Raetz, Ł. Bukowiecki, M. Kitze, R. Errmann, G. Nowak, A. Niedzielski, V. Popov, C. Marka, K. Goździewski, R. Neuhäuser, J. Ohlert, T. C. Hinse, J. W. Lee, C.-U. Lee, J.-N. Yoon, A. Berndt, H. Gilbert, C. Ginski, M. M. Hohle, M. Mugrauer, T. Röll, T. O. B. Schmidt, N. Tetzlaff, L. Mancini, J. Southworth, M. Dall'Ora, S. Ciceri, R. Zambelli, G. Corfini, H. Takahashi, K. Tachihara, J. M. Benkő, K. Sárneczky, G. M. Szabo, T. N. Varga, M. Vanko, Y. C. Joshi, and W. P. Chen. Multi-site campaign for transit timing variations of WASP-12 b: possible detection of

a long-period signal of planetary origin. , 551:A108, March 2013. doi: 10.1051/0004-6361/201220739.

G. Maciejewski, D. Dimitrov, M. Fernández, A. Sota, G. Nowak, J. Ohlert, G. Nikolov, Ł. Bukowiecki, T. C. Hinse, E. Pallé, B. Tingley, D. Kjurkchieva, J. W. Lee, and C.-U. Lee. Departure from the constant-period ephemeris for the transiting exoplanet WASP-12. , 588:L6, April 2016. doi: 10.1051/0004-6361/201628312.

K. Mandel and E. Agol. Analytic Light Curves for Planetary Transit Searches. , 580: L171–L175, December 2002. doi: 10.1086/345520.

T. Matsakos and A. Königl. A Hot Jupiter for Breakfast? Early Stellar Ingestion of Planets May Be Common. , 809:L20, August 2015. doi: 10.1088/2041-8205/809/2/L20.

M. Mayor and D. Queloz. A Jupiter-mass companion to a solar-type star. , 378:355–359, November 1995. doi: 10.1038/378355a0.

S. Meibom and R. D. Mathieu. A Robust Measure of Tidal Circularization in Coeval Binary Populations: The Solar-Type Spectroscopic Binary Population in the Open Cluster M35. , 620:970–983, February 2005. doi: 10.1086/427082.

J. Miralda-Escudé. Orbital Perturbations of Transiting Planets: A Possible Method to Measure Stellar Quadrupoles and to Detect Earth-Mass Planets. , 564:1019–1023, January 2002. doi: 10.1086/324279.

O. Neron de Surgy and J. Laskar. On the long term evolution of the spin of the Earth. , 318:975–989, February 1997.

J. D. Nichols, G. A. Wynn, M. Goad, R. D. Alexander, S. L. Casewell, S. W. H. Cowley, M. R. Burleigh, J. T. Clarke, and D. Bisikalo. Hubble Space Telescope Observations of the NUV Transit of WASP-12b. , 803:9, April 2015. doi: 10.1088/0004-637X/803/1/9.

G. I. Ogilvie. Tidal Dissipation in Stars and Giant Planets. , 52:171–210, August 2014. doi: 10.1146/annurev-astro-081913-035941.

G. I. Ogilvie and D. N. C. Lin. Tidal Dissipation in Rotating Solar-Type Stars. , 661: 1180–1191, June 2007. doi: 10.1086/515435.

A. Pál and B. Kocsis. Periastron precession measurements in transiting extrasolar planetary systems at the level of general relativity. , 389:191–198, September 2008. doi: 10.1111/j.1365-2966.2008.13512.x.

K. Penev, B. Jackson, F. Spada, and N. Thom. Constraining Tidal Dissipation in Stars from the Destruction Rates of Exoplanets. , 751:96, June 2012. doi: 10.1088/0004-637X/751/2/96.

K. Penev, J. D. Hartman, G. Á. Bakos, S. Ciceri, R. Brahm, D. Bayliss, J. Bento, A. Jordán, Z. Csubry, W. Bhatti, M. de Val-Borro, N. Espinoza, G. Zhou, L. Mancini, M. Rabus,

V. Suc, T. Henning, B. Schmidt, R. W. Noyes, J. Lázár, I. Papp, and P. Sári. HATS-18b: An Extreme Short-period Massive Transiting Planet Spinning Up Its Star. , 152:127, November 2016. doi: 10.3847/0004-6256/152/5/127.

E. S. Phinney. Pulsars as Probes of Newtonian Dynamical Systems. *Philosophical Transactions of the Royal Society of London Series A*, 341:39–75, October 1992. doi: 10.1098/rsta.1992.0084.

R. R. Rafikov. Stellar Proper Motion and the Timing of Planetary Transits. , 700:965–970, August 2009. doi: 10.1088/0004-637X/700/2/965.

R. R. Rafikov. On the Eccentricity Excitation in Post-main-sequence Binaries. , 830:8, October 2016. doi: 10.3847/0004-637X/830/1/8.

D. Ragozzine and A. S. Wolf. Probing the Interiors of very Hot Jupiters Using Transit Light Curves. , 698:1778–1794, June 2009. doi: 10.1088/0004-637X/698/2/1778.

F. A. Rasio, C. A. Tout, S. H. Lubow, and M. Livio. Tidal Decay of Close Planetary Orbits. , 470:1187, October 1996. doi: 10.1086/177941.

P. V. Sada, D. Deming, D. E. Jennings, B. k. Jackson, C. M. Hamilton, J. Fraine, S. W. Peterson, F. Haase, K. Bays, A. Lunsford, and E. O'Gorman. Extrasolar Planet Transits Observed at Kitt Peak National Observatory. , 124:212, March 2012. doi: 10.1086/665043.

D. D. Sasselov. The New Transiting Planet OGLE-TR-56b: Orbit and Atmosphere. , 596: 1327–1331, October 2003. doi: 10.1086/378145.

K. C. Schlaufman. Evidence of Possible Spin-orbit Misalignment Along the Line of Sight in Transiting Exoplanet Systems. , 719:602–611, August 2010. doi: 10.1088/0004-637X/719/1/602.

K. C. Schlaufman and J. N. Winn. Evidence for the Tidal Destruction of Hot Jupiters by Subgiant Stars. , 772:143, August 2013. doi: 10.1088/0004-637X/772/2/143.

D. K. Sing, A. Lecavelier des Etangs, J. J. Fortney, A. S. Burrows, F. Pont, H. R. Wakeford, G. E. Ballester, N. Nikolov, G. W. Henry, S. Aigrain, D. Deming, T. M. Evans, N. P. Gibson, C. M. Huitson, H. Knutson, A. P. Showman, A. Vidal-Madjar, P. A. Wilson, M. H. Williamson, and K. Zahnle. HST hot-Jupiter transmission spectral survey: evidence for aerosols and lack of TiO in the atmosphere of WASP-12b. , 436:2956–2973, December 2013. doi: 10.1093/mnras/stt1782.

K. B. Stevenson, J. L. Bean, A. Seifahrt, J.-M. Désert, N. Madhusudhan, M. Bergmann, L. Kreidberg, and D. Homeier. Transmission Spectroscopy of the Hot Jupiter WASP-12b from 0.7 to 5 μm. , 147:161, June 2014. doi: 10.1088/0004-6256/147/6/161.

S. Teitler and A. Königl. Why is there a Dearth of Close-in Planets around Fast-rotating Stars? , 786:139, May 2014. doi: 10.1088/0004-637X/786/2/139.

G. Torres, D. A. Fischer, A. Sozzetti, L. A. Buchhave, J. N. Winn, M. J. Holman, and J. A. Carter. Improved Spectroscopic Parameters for Transiting Planet Hosts. , 757:161, October 2012. doi: 10.1088/0004-637X/757/2/161.

F. Verbunt and E. S. Phinney. Tidal circularization and the eccentricity of binaries containing giant stars. , 296:709, April 1995.

E. Villaver and M. Livio. The Orbital Evolution of Gas Giant Planets Around Giant Stars. , 705:L81–L85, November 2009. doi: 10.1088/0004-637X/705/1/L81.

S. M. Wahl, W. B. Hubbard, and B. Militzer. Tidal Response of Preliminary Jupiter Model. , 831:14, November 2016. doi: 10.3847/0004-637X/831/1/14.

C. A. Watson and T. R. Marsh. Orbital period variations of hot Jupiters caused by the Applegate effect. , 405:2037–2043, July 2010. doi: 10.1111/j.1365-2966.2010.16602.x.

A. N. Wilkins, L. Delrez, A. J. Barker, D. Deming, D. Hamilton, M. Gillon, and E. Jehin. Searching for Rapid Orbital Decay of WASP-18b. , 836:L24, February 2017. doi: 10.3847/2041-8213/aa5d9f.

J. N. Winn. *Exoplanet Transits and Occultations*, pages 55–77. University of Arizona Press, December 2010.